NATIONAL ADVISORY COMMITTEE FOR AERONAUTICS

TECHNICAL NOTE 2245

CALCULATION OF COMPRESSIBLE POTENTIAL FLOW PAST SLENDER

BODIES OF REVOLUTION BY AN INTEGRAL METHOD

By Milton M. Klein and W. Perl

Lewis Flight Propulsion Laboratory
Cleveland, Ohio

NACA

Washington
December 1950

NATIONAL ADVISORY COMMITTEE FOR AERONAUTICS

TECHNICAL NOTE 2245

CALCULATION OF COMPRESSIBLE POTENTIAL FLOW PAST SLENDER

BODIES OF REVOLUTION BY AN INTEGRAL METHOD

By Milton M. Klein and W. Perl

SUMMARY

An integral method, previously used to obtain compressible flow past two-dimensional shapes, has been applied to the calculation of compressible potential flow past slender bodies of revolution. Good agreement of the resulting velocities on ellipsoids of revolution with those obtained by other methods was found. Flow-field conditions, such as the extent of local supersonic regions, were calculated and discussed. The free-stream Mach number beyond which a continuous potential-flow solution ceases to exist was found to be very close to 1.

INTRODUCTION

The partial differential equation for the compressible potential flow past a body of revolution is considerably more difficult to solve than the corresponding plane (two-dimensional) equation. As a consequence, fewer extensions of low-speed or incompressible-flow solutions to higher subsonic speeds have been made for bodies of revolution than for two-dimensional shapes. The principal work on bodies of revolution seems to have been confined to solutions of the partial differential equation after it has been linearized under the assumptions of small perturbations and of free-stream Mach number not too close to 1. For example, a treatment of subsonic flow by the method of sources and sinks is given in reference 1. The case of wholly supersonic flow, which has been more extensively treated, is discussed in reference 2. These solutions may be conveniently expressed in the form of a similarity rule (Prandtl-Glauert rule for bodies of revolution) that gives the flow pattern for a given Mach number if the flow pattern at another Mach number is known. Correct forms of the rule are presented in references 3 to 5.

The solution of the linearized differential equation yielding the Prandtl-Glauert rule may be regarded, as in the two-dimensional case, as the first term in an expansion of the potential in powers of a thickness-ratio parameter. The amount of labor required to obtain

higher-order terms of the expansion, is considerable for a two-dimensional body and much greater for the corresponding body of revolution. Only one calculation, for the ellipsoid of revolution, of the second term of such an expansion appears to have been made (reference 6).

Because of the large amount of work and the mathematical difficulties involved in obtaining higher approximations for bodies of revolution through the differential-equation approach, it is particularly desirable to survey other possible approaches to the problem of calculating the flow past a body of revolution at high subsonic Mach numbers. The integral-method approach of references 7 and 8 was therefore studied and the results of the investigation conducted at the NACA Lewis laboratory are presented herein.

The method of references 7 and 8 is based on an integral form of the equation of continuity and on the intrinsic form in terms of the local streamline curvature of the irrotationality condition. The essential approximation of the method is the choice of a curvature function that will adequately represent the variation of the streamline curvature in the flow field. In the two-dimensional problem, several guides are provided to limit the possible choices of a curvature function. These guides are: (a) the incompressible flow pattern; (b) the Prandtl-Glauert rule for the low-subsonic-speed range; and (c) the transonic similarity rule for the high-subsonic-speed range in which local supersonic regions exist in the flow field (references 9 and 10). For the axially symmetric case, guides (a) and (b) are available but the situation with regard to guide (c) is dubious.

An analysis of the differential equation for the body of revolution (reference 11) indicates that, although the transonic similarity rule of reference 9 may hold in the flow field, it does not appear to be valid on the body, where a different similarity rule obtains that is, moreover, valid only for extremely slender bodies. In this report, therefore, guide (c) has not been used in choosing a curvature function. The resulting greater arbitrariness of the choice of curvature function thus implies a greater uncertainty of results for bodies of revolution than for the two-dimensional shapes. In order to reduce this uncertainty, two substantially different curvature functions, both satisfying guides (a) and (b), have been selected for the investigation.

Although the illustrative examples given herein have been confined to ellipsoids of revolution, the method with either curvature function may be applied in a straightforward manner to arbitrary bodies of revolution.

ANALYSIS

The flow is assumed steady, isentropic, irrotational, and axially symmetric. Except for a modification in the continuity integral, the equations of motion and their development parallel the two-dimensional treatment of reference 8. The equations of motion are: (Main symbols are defined in the appendix; see fig. 1 for flow notation.)

Equation of continuity,

$$\int_0^{y_0} 2\pi y \rho_0 v_0 \, dy = \int_0^n 2\pi y \rho v \, dn \tag{1}$$

Irrotationality condition,

$$\frac{\partial v}{\partial n} + Cv = 0 \tag{2}$$

Bernoulli equation,

$$\frac{\rho}{\rho_0} = \left[1 - \frac{\gamma-1}{2} M_0^2 \left(\frac{v^2}{v_0^2} - 1 \right) \right]^{\frac{1}{\gamma-1}} \tag{3}$$

where

ρ density of fluid

v velocity in flow field

n distance measured along potential lines from body of revolution

C streamline curvature

γ ratio of specific heats

M Mach number

subscript 0 denotes free-stream conditions.

It is extremely simplifying to replace the coordinate n by the coordinate y in the preceding equations. Because of the dubious situation with regard to a transonic similarity rule, it does not appear

easy to give a rigorous justification for this replacement in the small-perturbation case analogous to the justification for the two-dimensional case given in appendix A of reference 8. The replacement of n by y, however, is exactly valid at the midchord location of bodies of revolution with fore-and-aft symmetry. The approximation involved in the replacement should therefore be fairly good near the maximum-thickness locations of slender bodies of revolution in general. For convenience, the free-stream quantities ρ_0 and v_0 will be taken as units of density and velocity so that ρ and v hereinafter represent non-dimensional fractions of free-stream density and velocity, respectively. In addition, the unit of length is taken as the airfoil chord, so that all lengths such as, x, y, and l/C hereinafter represent nondimensional fractions of the airfoil chord length.

Equations (1), (2), and (3) thus become, respectively,

$$\int_0^{y_0} y \, dy = \int_Y^y \rho v y \, dy \tag{4}$$

$$dy = \frac{dv}{Cv} \tag{5}$$

$$\rho = \left[1 - \frac{\gamma-1}{2} M_0^2 (v^2-1) \right]^{\frac{1}{\gamma-1}} \tag{6}$$

The variations indicated in equations (4) and (5) occur at constant x. The lower limit of integration Y in equation (4), which corresponds to the zero streamline, is the ordinate of the meridian section of the body of revolution. The variable upper limit y occuring in equation (4) and corresponding to the flow-field streamline may be eliminated by consideration of the limiting form of this equation as

$y \longrightarrow \infty$. In order to obtain a finite result, the quantity $\int_Y^y y \, dy$ is

subtracted from both sides of equation (4). If no wakes or sources of fluid exist in the flow field, then $\lim_{y \to \infty} (y-y_0) = 0$ (reference 8).

Equation (4) therefore assumes the limiting form, for $y \longrightarrow \infty$,

$$\frac{Y^2}{2} = \int_Y^\infty (\rho v - 1) \, y \, dy \tag{7}$$

The continuity equation (7) becomes, when dy is replaced by dv from equation (5),

$$\frac{Y^2}{2} = \int_1^V \left(\rho - \frac{1}{v} \right) \frac{y}{C} \, dv \tag{8}$$

in which the upper limit V is the velocity at the surface of the body corresponding to the ordinate Y. The relation between the flow-field velocity v and the corresponding distance y is obtained by integration of equation (5) between the limits Y and y as

$$y - Y = \int_V^V \frac{dv}{Cv} \tag{9}$$

For further simplification, the assumption of small perturbation of the flow velocity is now explicitly introduced; accordingly, the quantity $\rho - \frac{1}{v}$ in equation (8) is expressed as a power series in the velocity increment $\nu = v-1$. From equation (6), the quantity $\rho - \frac{1}{v}$ can be expanded in the form

$$\rho - \frac{1}{v} = \mu \nu - \Gamma_c \nu^2 + \Gamma_1 \nu^3 \tag{10}$$

where

$$\mu = 1 - M_0^2 \tag{11a}$$

$$\Gamma_c = 1 + \frac{M_0^2}{2} - \frac{2-\gamma}{2} M_0^4 \tag{11b}$$

$$\Gamma_1 = 1 + \frac{2-\gamma}{2} M_0^4 - \frac{1}{6} (2-\gamma)(3-2\gamma) M_0^6 \tag{11c}$$

Terms of higher order than v^3 in the expansion equation (10) are negligible in the solution to be derived herein. Substituting equation (10) into the continuity integral equation (8) and changing to a new variable of integration $z = v/\Lambda$ yield

$$\frac{Y^2}{2} = \Lambda^2 \int_0^1 (\mu z - \Gamma_c \Lambda z^2 + \Gamma_1 \Lambda^2 z^3) \frac{y}{C} \, dz \qquad (12)$$

where $\Lambda = V-1$ is the disturbance velocity on the body.

Equation (9) becomes, in terms of the new variable z,

$$y = Y + \Lambda \int_z^1 \frac{dz}{C(1+\Lambda z)} \qquad (13)$$

Inasmuch as $0 \leq z \leq 1$ and for small perturbations $\Lambda < < 1$, the quantity $\frac{1}{1+\Lambda z}$ may be expanded in powers of Λz, yielding

$$y = Y + \Lambda \int_z^1 \frac{1}{C} (1 - \Lambda z + \Lambda^2 z^2 - \Lambda^3 z^3 + \ldots) dz \qquad (14)$$

By inserting the value of y from equation (14) in equation (12), the continuity equation becomes, for arbitrary curvature C,

$$\frac{Y^2}{2} = \Lambda^2 \int_0^1 \left\{ \left(\mu z - \Gamma_c \Lambda z^2 + \Gamma_1^2 z^3 \right) \left[Y + \Lambda \int_z^1 \frac{1}{C} (1-\Lambda z+\Lambda^2 z^2-\Lambda^3 z^3 + \ldots) dz \right] \right\} \frac{dz}{C} \qquad (15)$$

First curvature function. - The streamline curvature is now assumed to be expressible as some simple function of the chosen independent variables, the chordwise location x, and the local velocity v. The function chosen must satisfy the boundary conditions of zero curvature at infinity and known curvature C_a on the body. Two curvature functions were chosen for investigation. The first curvature function is the same as that used for the two-dimensional problem (reference 8).

$$\frac{C}{C_a} = z^p \qquad (16)$$

where

C_a curvature of body contour

p parameter to be determined

The parameter p has a limited range of values because of conditions at infinity. The streamline curvature C must vanish at infinity and the integrals of equations (14) and (15) must diverge and converge, respectively, at the lower limit $z = 0$. Examination of equations (14) to (16) therefore shows that the parameter p must have the range of values (See also reference 7.)

$$1 \leq p < 3/2 \tag{17}$$

Substitution of equation (16) into equation (14) yields

$$y = Y + \frac{\Lambda}{C_a}\left[\frac{1-z^{1-p}}{1-p} - \Lambda\,\frac{(1-z^{2-p})}{2-p} + \Lambda^2\,\frac{(1-z^{3-p})}{3-p} - \Lambda^3\,\frac{(1-z^{4-p})}{4-p}\right] \tag{18}$$

The continuity integral equation (12) becomes, by use of equation (18),

$$\frac{Y^2}{2} = \frac{\Lambda^2}{C_a}\int_0^1 (\mu z^{1-p} - \Gamma_c\Lambda z^{2-p} + \Gamma_1\Lambda^2 z^{3-p})\left\{Y + \frac{\Lambda}{C_a}\left[\frac{1-z^{1-p}}{1-p} - \Lambda\,\frac{(1-z^{2-p})}{2-p} + \right.\right.$$

$$\left.\left. \Lambda^2\,\frac{(1-z^{3-p})}{3-p} - \Lambda^3\,\frac{(1-z^{4-p})}{4-p}\right]\right\}dz \tag{19}$$

Performing the integration and retaining terms through Λ^4 result in

$$\frac{(YC_a)^2}{2\Lambda^2} = \left(\frac{\mu}{2-p} - \frac{\Gamma_c\Lambda}{3-p} + \frac{\Gamma_1\Lambda^2}{4-p}\right)YC_a + \frac{\mu\Lambda}{(2-p)(3-2p)} - \left(\frac{\mu}{(2-p)(4-2p)} + \right.$$

$$\left. \frac{\Gamma_c}{(3-p)(4-2p)}\right)\Lambda^2 \tag{20}$$

Several terms in equation (20) are negligible throughout the entire subsonic range. Thus, of the terms involving YC_a as a factor, the term in Γ_1 is negligible when compared with the preceding one for $\Lambda \ll 1$. Of the terms not involving YC_a as a factor, the quantity in Λ^2 is negligible when compared with the term in $\mu\Lambda$ in the subsonic range $\mu \sim 1$, and in the Λ^2 terms, the term in μ is negligible compared with the term in Γ_c in the transonic range $\mu \sim 0$. Hence, the μ term within the second parenthesis on the right may be neglected and the continuity equation (20) becomes

$$\frac{(YC_a)^2}{2\Lambda^2} = \left(\frac{\mu}{2-p} - \frac{\Gamma_c\Lambda}{3-p}\right)YC_a + \frac{\mu\Lambda}{(2-p)(3-2p)} - \frac{\Gamma_c\Lambda^2}{(3-p)(4-2p)} \qquad (21)$$

Equation (21) provides the desired relation from which the velocity increment Λ may be obtained for given values of the free-stream Mach number M_0 and the curvature parameter of the body YC_a. Curves of Λ against $\sqrt{YC_a}$ for various values of M_0 and the parameter p are presented in figure 2. The numerical data from which these curves were drawn are presented in table I.

In applying equation (21), it is necessary first to obtain the parameter p. The parameter p is determined by requiring equation (21) to yield, in accordance with the discussion in the Introduction; (a) the known velocity Λ_i for incompressible flow $\mu = 1$, and (b) the Prandtl-Glauert rule for bodies of revolution in the low-subsonic-speed range ($\mu \sim 1$). For incompressible flow, the terms in Γ_c may be neglected and equation (21) becomes, with $\mu = 1$ and $\Lambda = \Lambda_i$,

$$\frac{(YC_a)^2}{2\Lambda_i^2} = \frac{YC_a}{2-p} + \frac{\Lambda_i}{(2-p)(3-2p)} \qquad (22)$$

The equation for determining p from the incompressible velocity Λ_i^0 and the body-curvature parameter YC_a is then, from equation (22)

$$p = \frac{7}{4} - \frac{\Lambda_i^2}{YC_a} - \sqrt{\frac{1}{16} + \frac{\Lambda_i^2}{YC_a}\left[\frac{\Lambda_i}{YC_a}(1+\Lambda_i) - \frac{1}{2}\right]} \qquad (23)$$

The minus sign is chosen for the square root because the value of p may not exceed $3/2$. In the low subsonic or Prandtl-Glauert range, the terms in Γ_c are still negligible and equation (21) has the form

$$\frac{(YC_a)^2}{2\Lambda^2} = \frac{\mu YC_a}{2-p} + \frac{\mu\Lambda}{(2-p)(3-2p)} \tag{24}$$

The quantity YC_a is of order τ^2, where τ is the thickness ratio. By multiplying the numerator and the denominator of the left side by μ^2, equation (24) may be expressed as

$$\mu\Lambda = f(\mu\tau^2, p) \tag{25}$$

The Prandtl-Glauert rule for bodies of revolution is (reference 1),

$$\mu\Lambda = g(\mu\tau^2, x) \tag{26}$$

where the function g is defined by the incompressible solution

$$\Lambda_i = g(\tau^2, x) \tag{27}$$

In order that equation (25) agree with the Prandtl-Glauert rule (equation (26)), the parameter p must be chosen as a function of $\mu\tau^2$ and x such that, for the incompressible case $\mu = 1$, this function reduces to that given in equation (23). Thus, in equation (23), τ^2 is to be replaced by $\mu\tau^2$ in determining p. The parameter p is thus a function of Mach number for bodies of revolution, in contrast to the two-dimensional case where it is constant. When the value of p is obtained from low-speed considerations, the velocity increment Λ at high subsonic speeds is determined from equation (21). The detailed method of application of equation (21) to the calculation of velocities at high subsonic Mach numbers will be discussed in the section APPLICATION TO ELLIPSOID OF REVOLUTION.

When the velocity increment Λ is determined, the local velocity υ at any distance y in the flow field may be obtained from equation (18), which becomes, on retention of terms through Λ^2,

$$y = Y + \frac{1}{p-1} \frac{\Lambda}{C_a} \left(\frac{1}{z^{p-1}} - 1 \right) - \frac{1}{2-p} \frac{\Lambda^2}{C_a} (1-z^{2-p}) \qquad (28)$$

The variation of streamline curvature C with distance y may then be obtained from equations (16) and (28).

Second curvature function. - As previously discussed, it was considered desirable to repeat the analysis with a second curvature function substantially different from the first. In this manner, the reliability of the solution could be assessed more accurately. For greater simplicity, the second curvature function was also chosen to eliminate the factor y in the integrand of the continuity integral equation (12). The second curvature function was therefore chosen as

$$\frac{C}{C_a} = z^q \frac{y}{Y} \qquad (29)$$

where the parameter q is to be determined as a function of x from the same low-speed considerations used to determine the parameter p in the preceding section. By an analysis similar to that used to determine the permissible values of p, the range of values of q is (reference 7),

$$1 \leq q < 2 \qquad (30)$$

Substituting equation (29) into the continuity equation (12), integrating, and retaining terms through Λ^3 yield

$$\frac{YC_a}{2} = \frac{\mu\Lambda^2}{2-q} - \frac{\Gamma_c\Lambda^3}{3-q} \qquad (31)$$

Equation (31) provides the basic relation from which the velocity increment Λ may be calculated for given values of M_0 and YC_a. For incompressible flow, the term in Γ_c is negligible so that the parameter q is determined from

$$\frac{YC_a}{2} = \frac{\Lambda_1^2}{2-q} \qquad (32)$$

In the Prandtl-Glauert range, the term in Γ_c is still negligible, so that equation (31) becomes

$$\frac{YC_a}{2} = \frac{\mu\Lambda^2}{2-q} \tag{33}$$

In order that equation (33) agree with the Prandtl-Glauert rule for bodies of revolution (equation (26)) the parameter q is chosen as a function of $\mu\tau^2$ and x such that for the incompressible case this function reduces to equation (32). The velocity increment Λ is then determined at high subsonic speeds from equation (31), which may be conveniently solved by introducing two new parameters λ and χ (reference 9). When λ and χ are defined by

$$\lambda = \left(\frac{2-q}{3-q}\right)\frac{\Gamma_c}{\mu}\Lambda \tag{34a}$$

$$\chi = \frac{YC_a}{2}\frac{\Gamma_c^2}{\mu^3}\frac{(2-q)^3}{(3-q)^2} \tag{34b}$$

equation (31) assumes the form

$$\chi = \lambda^2 - \lambda^3 \tag{35}$$

A plot of equation (35) is presented in figure 3; the significance of the vertical tangents in figures 2 and 3 and their relation to the so-called potential-limit phenomenon are discussed in references 7 and 8.

After the velocity increment Λ on the body is obtained, the local velocity increment v at any distance y in the flow field can be obtained by means of equation (5). Introducing equation (29) into equation (5) and changing over to the variable z yield

$$\int_Y^y y\, dy = \frac{Y\Lambda}{C_a}\int_z^1 \frac{dz}{z^q(1+\Lambda z)} \tag{36}$$

Expanding the quantity $1/1+\Lambda z$, integrating term by term, and retaining terms through Λ^2 give

$$y^2 - Y^2 = \frac{2Y\Lambda}{C_a} \frac{1}{q-1} \left(\frac{1}{z^{q-1}} - 1 \right) - \frac{2Y\Lambda^2}{C_a} \frac{1}{2-q} (1-z^{2-q}) \qquad (37)$$

The variation of streamline curvature with distance y may then be obtained from equations (29) and (37).

APPLICATION TO ELLIPSOID OF REVOLUTION

As an illustration of the foregoing analysis, the velocity distribution on an ellisoid of revolution at high subsonic Mach numbers will be calculated. The incompressible velocity distribution for an ellisoid of revolution of thickness ratio τ may be obtained from the expression for the velocity potential given in reference 12 and is given by

$$1 + \Lambda_i = \left[1 + f(\tau) \right] \sqrt{\frac{1-\xi^2}{1-\xi^2(1-\tau^2)}} \qquad (38)$$

where

$$f(\tau) = \frac{\tau^2 \log_e \frac{1+\sqrt{1-\tau^2}}{1-\sqrt{1-\tau^2}} - 2\tau^2\sqrt{1-\tau^2}}{2\sqrt{1-\tau^2} - \tau^2 \log_e \frac{1+\sqrt{1-\tau^2}}{1-\sqrt{1-\tau^2}}} \qquad (39)$$

ξ chordwise location measured from center of ellipsoid, semichords.

The curvature parameter YC_a for an ellipse is given by

$$YC_a = \frac{\tau^2 \sqrt{1-\xi^2}}{\left[1-\xi^2(1-\tau^2)\right]^{3/2}} \qquad (40)$$

First curvature function. - The parameter p is determined from equation (23) using the values of Λ_i and YC_a from equations (38) and (40), respectively. Although not so determined herein, the value of p may also be obtained directly from the curves of figure 2 for $M_0 = 0$. In accordance with the discussion on the Prandtl-Glauert rule, p is to be determined as a function of $\mu\tau^2$, which reduces to the

known dependence of p on τ^2 for incompressible flow ($\mu = 1$). The variation of p with μ is conveniently obtained by plotting p against τ^2 and changing the abscissa designation to $\mu\tau^2$. The variation of p with $\mu\tau^2$ for several chordwise locations is presented in figure 4. The values of p increase with increasing distance from the center of the body and approach a limiting value of $3/2$. The occurrence of this limiting value may be seen by noting that the incompressible velocity Λ_i passes through zero near the trailing edge and, from equation (23), the parameter p approaches $3/2$ as Λ_i approaches zero. Having obtained the value of p at the Mach number M_0, the velocity increment Λ for a given YC_a is then obtained from the basic graphs of figure 2. Except for the additional step of finding p as a function of Mach number, the procedure is essentially the same as that given in reference 7.

The parameter p has a limiting value of $3/2$ for either $\Lambda_i \longrightarrow 0$ or $\mu \longrightarrow 0$. The graphical procedure for obtaining p therefore tends to become somewhat inaccurate at high Mach numbers unless great care is used, especially at those locations off the center where the velocity is close to zero. The value of p was therefore analytically determined at the higher Mach numbers. Because the value of p at a Mach number M_0 is the same as the incompressible value of p for a thickness ratio reduced by the factor $\sqrt{\mu}$, only higher-order terms were retained. Inasmuch as for $p \longrightarrow 3/2$, $2-p \longrightarrow \frac{1}{2}$, equation (22) becomes, on retention of higher-order terms,

$$3-2p = \frac{4\Lambda_i{}^3}{(YC_a)^2} \tag{41}$$

Equation (38) becomes, on retaining terms in $f(\tau)$ through τ^2,

$$1 + \Lambda_i = \left[1 + \frac{\tau^2}{2}\left(\log_e \frac{4}{\tau^2} - 2\right)\right] \sqrt{\frac{1-\xi^2}{1-\xi^2(1-\tau^2)}} \tag{42}$$

Substituting equations (40) and (42) in equation (41) and replacing τ^2 by $\mu\tau^2$ yields, for p as a function of Mach number,

$$3-2p = 4\left\{\left[1 + \frac{\mu\tau^2}{2}\left(\log_e \frac{4}{\mu\tau^2} - 2\right)\right] \sqrt{\frac{1-\xi^2}{1-\xi^2(1-\mu\tau^2)}} - 1\right\}^3 \frac{\left[1-\xi^2(1-\mu\tau^2)\right]^3}{\mu^2\tau^4(1-\xi^2)} \tag{43}$$

The velocity increment Λ was then found in the usual manner with the aid of the basic graphs (fig. 2). The procedure involving the analytical determination of p was used in the range $M_0 \geq 0.95$.

Second curvature function. - The parameter q is determined by means of equation (32) using the values of Λ_1 and YC_a from equations (38) and (40), respectively. The variation of q with Mach number is then obtained by plotting q against τ^2 and changing the abscissa designation to $\mu\tau^2$. The variation of q with $\mu\tau^2$ for several chordwise locations is also presented in figure 4; the values of q are closer to the limiting value of 2 for the larger chordwise locations. When the value of q at the Mach number M_0 is obtained, the parameter X is then calculated from equation (34b). The value of the parameter λ is next obtained from the λ, X curve of figure 3. The velocity increment Λ is finally obtained from equation (34a). Except for the additional step of finding q as a function of Mach number, the procedure is essentially the same as that of reference 8. It may be noted that calculations with the second curvature function are simpler than those with the first curvature function.

As for the first curvature function, it is preferable to determine analytically the parameter q at high Mach numbers. Substituting equations (40) and (42) in equation (32) and replacing τ^2 by $\mu\tau^2$ yields, for q as a function of Mach number,

$$2-q = 2\left\{\left[1 + \frac{\mu\tau^2}{2}\left(\log_e \frac{4}{\mu\tau^2} -2\right)\right] \sqrt{\frac{1-\xi^2}{1-\xi^2(1-\mu\tau^2)}}\right\}^2 \frac{\left[1-\xi^2(1-\mu\tau^2)\right]^{3/2}}{\mu\tau^2\sqrt{1-\xi^2}} \quad (44)$$

The velocity increment Λ is then obtained by the procedure following the graphical determination of q. The procedure involving the analytical determination of q was used for Mach numbers $M_0 \geq 0.95$.

RESULTS AND DISCUSSION

The methods developed herein for both curvature functions have been used to calculate velocity distributions on ellipsoids of revolution and conditions in the flow field for several thickness ratios and a range of Mach numbers. The variation of the maximum velocity increment Λ_{max} at the center of the ellipsoid with free-stream Mach number M_0 for several thickness ratios is presented in figure 5. In order to indicate the local Mach number M corresponding to a given velocity increment Λ, contours of local Mach number obtained from

the Bernoulli relation between velocity increment Λ, local Mach
number M, and free-stream Mach number M_0 have been plotted on
the figure. For the purpose of comparison, the values given in ref-
erence 6 and the values given by the Prandtl-Glauert rule (equations
(26), (27), and (38)) are also included. For purposes of comparison,
the Prandtl-Glauert rule is shown in figure 5 for local Mach numbers
greater than 1, although this procedure is, strictly speaking, not
permissible. On the whole, good agreement among the various methods
is indicated.

The velocity distribution on the body for several thickness ratios
and Mach numbers is presented in figure 6. These distributions have
been terminated at the values of ξ for which Λ passes through zero
because the curvature functions chosen for this investigation, inasmuch
as they yield positive values of the streamline curvature, may not be
used for negative velocity increments. The agreement between the two
curvature functions in figure 6 is essentially the same as that indi-
cated in figure 5. The $M_{0,l}$ curves in figure 6 will be discussed
in the section POTENTIAL LIMIT.

The results with regard to the flow field are presented in fig-
ures 7 to 9. The variation of the velocity parameter z with lateral
distance $y-\tau$ is given in figure 7. The curvature C/C_a is plotted
as a function of $y-\tau$ in figure 8 and as a function of z in fig-
ure 9. In contrast to the fairly good agreement for the velocity dis-
tributions on the body, the results in the flow field are not in good
agreement. This behavior is plausible inasmuch as the procedure for
determining the curvature function utilizes the velocities on the body
in the Prandtl-Glauert speed range as reference values. Thus, whereas
the method used herein to determine the curvature function can be
regarded as averaging out local differences in the areas under the
C/C_a against $y-\tau$ curves in figure 8 to yield about the same surface
velocities (in accordance with equation (5)), the local differences in
the flow field may be substantial.

It is shown in figures 8 and 9 that the two curvature functions
are quite different in type, as is evidenced by the values of C/C_a
greater than 1 exhibited by the second curvature function at high Mach
numbers and low thickness ratios. Inasmuch as the curvature C/C_a
should probably not exceed 1, this phenomenon may be regarded as a
criterion for eliminating this type of curvature function from consider-
ation. The results obtained by the first curvature function are there-
fore probably more reliable than those obtained by the second curvature
function.

The lateral and longitudinal extents of the symmetric-type local supersonic regions that develop at the higher Mach numbers, y_s-τ and ξ_s, are presented as functions of free-stream Mach number in figures 10 and 11, respectively. These values were obtained from the velocities in the flow field (fig. 7), the velocity distribution on the body (fig. 6), and the local $M = 1$ contour of figure 5. The two curvature functions are not in good agreement with regard to lateral extent of the local supersonic region, the discrepancy becoming more evident with decreasing thickness ratio. The two curvature functions are in much better agreement with respect to chordwise extent of the supersonic region, a result to be anticipated in view of the good agreement of the velocity distributions on the body (fig. 6). In order to indicate the differences between two-dimensional and axially symmetric flow with regard to extent of the supersonic region, the results for the elliptic cylinder, calculated by the method of reference 8 are included in figures 10 and 11. Although the supersonic region starts at a much higher Mach number for the ellipsoid of revolution than for the elliptic cylinder, the lateral extent y_s-τ attains much higher values for the ellipsoid of revolution than for the elliptic cylinder.

POTENTIAL LIMIT

The calculation of two-dimensional compressible flows by the integral method (references 7 and 8) yields a free-stream Mach number, called the potential-limit Mach number $M_{0,l}$, beyond which, for a given thickness ratio, a continuous solution for the whole body cannot be obtained. The same phenomenon is found to occur in the treatment of bodies of revolution by the present method. The potential-limit Mach number corresponds to the points of vertical tangency of the Λ against $\sqrt{YC_a}$ curves of figure 2 or of the λ against X curve of figure 3. The value of $M_{0,l}$ for the curvature functions investigated herein may therefore be obtained by application of the conditions

$$\left(\frac{\partial \sqrt{YC_a}}{\partial \Lambda} \right)_{M_0} = 0 \qquad\qquad (45)$$

$$\frac{dX}{d\lambda} = 0 \qquad\qquad (46)$$

to equations (21) and (35), respectively. For the first curvature

function there is obtained

$$
YCa = - \frac{\Lambda}{2-p} \frac{\left(\dfrac{3\mu}{3-2p} - \dfrac{2\Gamma_c}{3-p} \Lambda \right)}{\left(\dfrac{2\mu}{2-p} - \dfrac{3\Gamma_c}{3-p} \Lambda \right)} \tag{47}
$$

and for the second curvature function the result is

$$
\lambda = \left(\frac{2-q}{3-q} \right) \frac{\Gamma_c \Lambda}{\mu} = \frac{2}{3} \tag{48}
$$

For the ellipsoid of revolution and, probably more generally, for aerodynamic shapes, the potential limit occurs at the midchord section. (See reference 7 for discussion of two-dimensional case.) The potential-limit values of μ and Λ for the first curvature function were obtained by simultaneous solution of equations (21) and (47) at the midchord location. Because of the variation of the parameter p with Mach number and the complicated form of the continuity equation (21), the work was considerably more difficult than for the corresponding two-dimensional problem. It was found convenient to adopt an iteration procedure in which the values of μ were obtained from the continuity equation (21) and the corresponding values of Λ from the potential-limit equation (47). The parameter p was determined from the simplified equation (43) evaluated at the midchord location, $\xi = 0$. Initial values of μ and Λ for the iteration were obtained as follows:

At the potential limit, the value of μ is small so that the parameter p is close to its limiting values of 3/2. The continuity equation (21) and the potential-limit equation (47) may therefore be approximated by, respectively,

$$
\frac{\mu}{3-2p} = \frac{(YCa)^2}{4\Lambda^3} + \frac{1}{3} \Gamma_c(YCa+\Lambda) \tag{49}
$$

$$
\frac{\mu}{3-2p} = \frac{\Gamma_c}{3} \left(YCa + \frac{4}{3} \Lambda \right) \tag{50}
$$

Equating the right sides of equations (49) and (50) yields

$$\Lambda = \left(\frac{3}{2}\right)^{\frac{1}{2}} \left(\frac{1}{\Gamma_c}\right)^{\frac{1}{4}} \sqrt{YC_a} \tag{51}$$

The value of Γ_c at the potential limit is close to its limiting value of 1.2 for $M_0 = 1$. Taking $\Gamma_c = 1.2$, the value of Λ_l may then be obtained from equation (51) and the value of μ_l, from either equation (49) or (50). The initial values of μ_l and Λ_l were within a few percent of the final iterated values. After the potential-limit Mach number $M_{0,l}$ is obtained, the velocity distribution on the body and in the flow field can be calculated in the usual manner.

For the second curvature function, the potential-limit values of μ and Λ may be more directly obtained. Insertion of equation (48) into equation (35) yields

$$\chi = \frac{YC_a}{2} \frac{\Gamma_c^2}{\mu^3} \frac{(2-q)^3}{(3-q)^2} = \frac{4}{27} \tag{52}$$

where the parameter q is given by the simplified equation (44) evaluated at $\xi = 0$. The quantity μ_l was then obtained from a plot of the parameter χ against μ and the corresponding value of Λ_l, from equation (48).

The velocity distribution on the body at the potential limit is given in figure 6. The velocity gradient at the midchord exhibits, as in the case of two-dimensional flow, a finite discontinuity (reference 7). The results for the flow field at the potential limit are given in figures 12 to 14. The discrepancies previously noted between the two curvature functions become even more evident at the potential limit. The extreme maximum values of C/C_a exhibited by the second curvature function indicate that it is probably very inaccurate near the potential limit. The potential-limit values of the lateral and longitudinal extents of the local supersonic region are indicated by circles in figures 10 and 11. (Some potential limit values of y_s-τ are outside range of fig. 10.)

The variation of the potential-limit values of free-stream Mach number and maximum velocity increment with thickness ratio is given in figure 15 and the lateral and longitudinal extents of the super-sonic region at the potential limit as a function of thickness ratio

in figure 16. For comparison, the corresponding curves for the ellip-
tic cylinder are also presented in figures 15 and 16. The potential-
limit Mach number $M_{0,l}$ is much higher for the ellipsoid of revolu-
tion than for the elliptic cylinder and is very close to 1. These high
values of $M_{0,l}$ may be interpreted as follows: A body of revolution
produces a smaller relative decrease of cross-sectional area between
the body streamline A-A and an arbitrary streamline B-B (fig. 1)
than the corresponding two-dimensional shape. The consequent smaller
velocity increments for the body of revolution result in higher values
of the free-stream Mach number at which the supersonic region has
started to develop (lower critical Mach number). Thus, it is plausible
that the potential limit will occur at a much higher free-stream Mach
number for the body of revolution than for the corresponding two-
dimensional shape. It is surprising, however, that the values of $M_{0,l}$
are as close to 1 for a body of revolution as is indicated by the
present method. The values of $M_{0,l}$ for the second curvature function
are higher than those for the first curvature function. The difference
in $M_{0,l}$ for the two curvature functions may be explained on the basis
of the large values of curvature exhibited by the second curvature
function (figs. 8 and 13). These large values of curvature lead to a
rapid decrease of velocity with distance from the body (equation (5)).
It is therefore to be expected that the lateral extent of the local
supersonic region at a given Mach number would be smaller for the
second curvature function than for the first curvature function.
(Fig. 10 verifies this conclusion.) It then follows that the flow
described by the second curvature function will not attain the maximum
value of M_0 beyond which a symmetric-type solution may not be con-
tinued (reference 7) until the flow given by the first curvature
function has done so.

The variation of maximum velocity increment at the potential limit
$\Lambda_{max,l}$ with thickness ratio τ for the first curvature function is
approximately linear and close to that given by the initial choice of
$\Lambda_{max,l}$ for iteration previously discussed (equation (51)). The vari-
ation of $\Lambda_{max,l}$ with τ for the second curvature function is of the
2/3 power type, as may be seen from equation (48) and (52). This vari-
ation, however, is the same as that given by the similarity law for two-
dimensional flow (references 8 and 9), and illustrated by the curve of
$\Lambda_{max,l}$ against τ for the elliptic cylinder. The description of
$\Lambda_{max,l}$ by the second curvature function is therefore to be regarded
as another of its inaccuracies.

The lateral extent of the supersonic region at the potential limit
is much greater for the ellipsoid of revolution than for the elliptic
cylinder. The extreme extent of the supersonic region for the ellipsoid
of revolution is largely due to the closeness of $M_{0,l}$ to 1. For
values of free-stream Mach number near 1, the disturbance velocity

decays very slowly with lateral distance from the body (reference 13).
In addition, a very small velocity increment is needed to yield sonic
velocity. The lateral extent of the supersonic region should there-
fore rise very rapidly in the neighborhood of the potential limit.
(See figs. 10 and 16.) The extreme behavior of the flow field in the
neighborhood of the potential limit indicated by the present method
may therefore be reasonable for potential flow. It is, of course,
possible that the symmetric-type flow given by the present method
would be terminated by a shock before such extreme sizes of the super-
sonic region are attained.

On the basis of steady-state considerations, the potential-limit
Mach number $M_{0,l}$ is interpreted in reference 8 as the transition Mach
number between symmetric-type solutions for $M_0 < M_{0,l}$ and asymmetric-
type solutions for $M_0 > M_{0,l}$, with a shock terminating the symmetric-
type solution. The extreme closeness of $M_{0,l}$ to 1 would therefore
indicate that the drag-divergence Mach number associated with the
strong shock that terminates the symmetric-type local supersonic
region should occur much closer to 1 for bodies of revolution than for
the corresponding two-dimensional shapes.

CONCLUDING REMARKS

An integral method has been extended to obtain the compressible
potential flow past a body of revolution. Of the two curvature func-
tions chosen for the investigation, the first curvature function appears
more reliable than the second curvature function.

Although the symmetric-type local supersonic region first appears
at a much higher Mach number for the ellipsoid of revolution than for
the elliptic cylinder, it attains a much greater lateral extent. The
potential-limit Mach number is much higher for the ellipsoid of revolu-
tion than for the elliptic cylinder and very close to 1. The Mach
number for drag divergence should therefore occur at a Mach number much
closer to 1 for a body of revolution than for the corresponding two-
dimensional shape. The present approach offers fairly simple methods
for calculating the velocity distribution on a body of revolution at
high subsonic Mach numbers with local supersonic regions.

Lewis Flight Propulsion Laboratory,
    National Advisory Committee for Aeronautics,
        Cleveland, Ohio, September 1, 1950.

APPENDIX - SYMBOLS

The following symbols are used in this report:

C   streamline curvature

M   Mach number

n   distance measured along potential lines from body of revolution

p,q parameters for curvature functions

V   resultant velocity on body of revolution

v   velocity in flow field

x   distance along axis of body of revolution measured from leading edge

Y   ordinate of meridian section of body of revolution

y   lateral distance normal to free-stream direction

$z = \upsilon/\Lambda$

$\Gamma_c = 1 - \dfrac{M_0{}^2}{2} - \dfrac{2-\gamma}{2} M_0{}^4$

γ ratio of specific heats

Λ velocity increment, V-1

$\lambda = \dfrac{(2-q)}{(3-q)} \dfrac{\Gamma_c}{\mu} \Lambda$

$\mu = 1-M_0{}^2$

υ velocity increment, v-1

ξ distance along axis of body of revolution measured from center, semichord

ρ density of fluid

τ thickness ratio

$\chi = \dfrac{YC_a}{2} \dfrac{\Gamma_c{}^2}{\mu^3} \dfrac{(2-q)^3}{(3-q)^2}$

Subscripts:

a   at surface of body of revolution

i   incompressible or low-speed value

l potential limit

s   sonic value

0   free-stream condition

REFERENCES

1. Bilharz, Herbert, and Hölder, Ernst: Calculation of the Pres-
    sure Distribution on Bodies of Revolution in the Subsonic Flow
    of a Gas. Part I - Axially Symmetrical Flow. NACA TM 1153,
    1947.

2. von Kármán, Theodor, and Moore, Norton B.: Resistance of Slender
    Bodies Moving with Supersonic Velocities, with Special Refer-
    ence to Projectiles. Trans. A.S.M.E., vol. 54, no. 23,
    Dec. 15, 1932, pp. 303-310.

3. Sears, W. R.: A Second Note on Compressible Flows about Bodies
    of Revolution. Quart. Appl. Math., vol. 5, no. 1, April 1947,
    pp. 89-91.

4. Hess, Robert V., and Gardner, Clifford S.: Study by the Prandtl-
    Glauert Method of Compressibility Effects and Critical Mach
    Number for Ellipsoids of Various Aspect Ratios and Thickness
    Ratios. NACA TN 1792, 1949.

5. Lees, Lester: A Discussion of the Application of the Prandtl-
    Glauert Method to Subsonic Compressible Flow over a Slender
    Body of Revolution. NACA TN 1127, 1946.

6. Schmieden, C., and Kawalki, K. H.: Contribution to the Problem
    of Flow at High Speed. NACA TM 1233, 1949.

7. Perl, W.: Calculation of Compressible Flows past Aerodynamic
    Shapes by Use of the Streamline Curvature. NACA TN 1328, 1947.

8. Perl, William: Calculation of Transonic Flows past Thin Airfoils
    by an integral Method. NACA TN 2130, 1950.

9. von Kármán, Theodor: The Similarity Law of Transonic Flow. Jour.
    Math. Phys., vol. XXVI, Oct. 1947, pp. 182-190.

10. Guderly, K. Gottfried: Considerations of the Structure of Mixed
    Subsonic-Supersonic Flow Patterns. Tech. Rep. No. F-TR-2168-ND,
    Tech. Intell., Air Material Command (Wright Field), Oct. 1947.

11. Perl, W., and Klein, Milton M.: Theoretical Investigation of
    Transonic Similarity for Bodies of Revolution.
    NACA TN 2239, 1950.

12. Lamb, Horace: Hydrodynamics. Dover Pub., 6th ed., 1945, p. 141.

13. Sauer, Robert: Introduction to Theoretical Gas Dynamics.
    J. W. Edwards (Ann Arbor), 1947, p. 51.

TABLE I – BASIC CALCULATIONS FOR OBTAINING VELOCITY INCREMENT Λ (EQUATION (21))

[First curvature function, $C/C_a = zP$.]

NACA

Note: $\sqrt{YC_a}$ marks the cutoff boundary (located near the 0.25 column band).

M_0	p	Λ 0.02	0.04	0.06	0.08	0.10	0.12	0.16	0.20	0.25	0.30	0.40	0.50	0.60	0.70	0.80	0.90	1.0
0	1.0	0.0665	0.1138	0.1563	0.1960	0.2338	0.2702	0.3396	0.4055	0.4841	0.5592	0.7006	0.8315	0.9530	1.0656	1.1693		
	1.1	.0718	.1230	.1689	.2118	.2526	.2918	.3666	.4377	.5225	.6037	.7567	.8991	1.0319	1.1558			
	1.2	.0792	.1355	.1859	.2329	.2776	.3206	.4025	.4804	.5752	.6623	.8305	.9877	1.1352	1.2735			
	1.3	.0895	.1538	.2109	.2639	.3144	.3628	.4550	.5428	.6471	.7474	.9370	1.1148	1.2830				
	1.4	.1099	.1881	.2570	.3210	.3818	.4399	.5506	.6555	.7807	.9004	1.1276						
	1.45	.1344	.2260	.3086	.3848	.4569	.5259	.6568	.7806	.9280	1.0691	1.3363						
	1.48	.1688	.2855	.3886	.4838	.5736	.6593	.8217	.9749	1.1569								
	1.495	.2389	.4029	.5473	.6802	.8053	.9247	1.1499										
	1.499	.3567	.6005	.8146	1.0118													
	1.4999	.6331	1.0652															
0.4	1.0	0.0628	0.1082	0.1483	0.1857	0.2213	0.2553	0.3200	0.3811	0.4534	0.5221	0.6498	0.7660	0.8715	0.9666	1.0515		
	1.1	.0688	.1169	.1604	.2009	.2392	.2760	.3459	.4120	.4903	.5650	.7038	.8313	.9479	1.0545			
	1.2	.0756	.1290	.1766	.2210	.2632	.3036	.3803	.4529	.5393	.6213	.7752	.9170	1.0482	1.1694			
	1.3	.0852	.1466	.2007	.2508	.2985	.3441	.4308	.5128	.6102	.7033	.8782	1.0406					
	1.4	.1048	.1795	.2449	.3057	.3633	.4183	.5228	.6217	.7392	.8514	1.0630						
	1.45	.1284	.2158	.2944	.3669	.4354	.5009	.6250	.7423	.8816	1.0144							
	1.48	.1614	.2729	.3712	.4621	.5476	.6292	.7837	.9392									
	1.495	.2286	.3854	.5234	.6505	.7699	.8838	1.0988										
	1.499	.3413	.5745	.7795	.9680													
	1.4999	.6061	1.0194															
0.6	1.0	0.0584	0.1000	0.1369	0.1709	0.2032	0.2339	0.2919	0.3462	0.4099	0.4694	0.5776	0.6725	0.7549	0.8246	0.8798	0.9257	0.9563
	1.1	.0634	.1083	.1482	.1851	.2200	.2533	.3162	.3752	.4445	.5095	.6287	.7347	.8284	.9098	.9794	1.0367	1.0817
	1.2	.0700	.1197	.1634	.2040	.2424	.2791	.3485	.4137	.4904	.5628	.6963	.8168	.9249	1.0217	1.1067	1.1807	1.2430
	1.3	.0793	.1359	.1859	.2319	.2755	.3171	.3959	.4701	.5577	.6405	.7945	.9350	1.0636	1.1811	1.2876	1.3838	1.4694
	1.4	.0976	.1668	.2273	.2854	.3364	.3869	.4827	.5729	.6796	.7810	.9707	1.1463	1.3092	1.4615	1.6031	1.7355	1.8580
	1.45	.1197	.2009	.2738	.3409	.4042	.4647	.5790	.6867	.8143	.9356	1.1632	1.3755	1.5742	1.7618	1.9388	2.0164	2.2652
	1.48	.1506	.2543	.3458	.4301	.5182	.5851	.7282	.8628	1.0223								
	1.495	.2134	.3596	.4883	.6066	.7178	.8238	1.0238										
	1.499	.3187	.5366	.7278	.9037													
	1.4999	.5661	.9523															
0.7	1.0	0.0551	0.0939	0.1281	0.1596	0.1893	0.2176	0.2705	0.3196	0.3764	0.4290	0.5221	0.6003	0.6642	0.7131	0.7469	0.7647	0.7658
	1.1	.0596	.1017	.1387	.1730	.2052	.2359	.2935	.3471	.4095	.4672	.5713	.6607	.7362	.7978	.8455	.8789	.8976
	1.2	.0662	.1122	.1531	.1909	.2265	.2604	.3241	.3837	.4533	.5183	.6364	.7401	.8305	.9081	.9727	1.0245	1.0633
	1.3	.0747	.1278	.1744	.2174	.2579	.2965	.3692	.4374	.5175	.5926	.7308	.8548	.9659	1.0448	1.1520	1.2277	1.2919
	1.4	.0920	.1570	.2137	.2662	.3156	.3628	.4518	.5554	.6340	.7271	.9004	1.0589	1.2047	1.3389	1.4534	1.5754	1.6785
	1.45	.1129	.1893	.2578	.3207	.3801	.4367	.5435	.6439	.7626	.8749	1.0852	1.2796	1.4609	1.6304	1.7893	1.9383	2.0779
	1.48	.1421	.2399	.3260	.4053	.4799	.5510	.6853	.8114	.9605								
	1.495	.2015	.3396	.4609	.5636	.6772	.7771	.9654										
	1.499	.3011	.5068	.6873	.8532	1.0091												
	1.4999	.5549	.8996	1.1948														
0.8	1.0	0.0509	0.0852	0.1157	0.1437	0.1699	0.1946	0.2404	0.2821	0.3294	0.3716	0.4424	0.4950	0.5287	0.5419	0.5324	0.4965	0.4287
	1.1	.0546	.0920	.1256	.1560	.1845	.2115	.2616	.3076	.3601	.4078	.4896	.5541	.6016	.6313	.6424	.6336	.6033
	1.2	.0603	.1019	.1387	.1725	.2041	.2341	.2901	.3417	.4011	.4556	.5516	.6314	.6956	.7440	.7768	.7935	.7940
	1.3	.0683	.1162	.1583	.1969	.2332	.2675	.3319	.3917	.4611	.5256	.6416	.7421	.8281	.9005	.9915	1.0047	1.0371
	1.4	.0842	.1431	.1945	.2419	.2865	.3289	.4086	.4830	.5701	.6519	.8021	.9371	1.0587				
	1.45	.1032	.1728	.2351	.2922	.3460	.3972	.4935	.5837	.6899	.7901	.9760						
	1.48	.1300	.2193	.2978	.3708	.4381	.5027	.6245	.7387	.8736	1.0011							
	1.495	.1845	.3108	.4217	.5237	.6194	.7106	.8824	1.0436									
	1.499	.2759	.4642	.6296	.7815	.9241												
	1.4999	.4502	.8244	1.1178														
0.85	1.0	0.0459	0.0790	0.1072	0.1327	0.1566	0.1789	0.2196	0.2561	0.2963	0.3311	0.3844	0.4151	0.4201	0.3933	0.3206	0.1445	0.2892
	1.1	.0507	.0855	.1164	.1444	.1704	.1948	.2398	.2804	.3260	.3661	.4312	.4759	.4995	.4993	.4716	.4101	.2992
	1.2	.0560	.0949	.1288	.1599	.1889	.2161	.2667	.3129	.3652	.4124	.4923	.5539	.5972	.6219	.6269	.6111	.5731
	1.3	.0635	.1083	.1474	.1829	.2162	.2477	.3064	.3605	.4226	.4797	.5800	.6635	.7313	.7859	.8205	.8423	.8490
	1.4	.0786	.1336	.1814	.2253	.2666	.3057	.3790	.4472	.5266	.6006	.7349	.8536	.9583	1.0500			
	1.45	.0965	.1615	.2195	.2727	.3227	.3701	.4593	.5426	.6403	.7321	.9013	1.0548	1.1945				
	1.48	.1217	.2051	.2785	.3459	.4093	.4695	.5828	.6889	.8139	.9319							
	1.495	.1728	.2910	.3947	.4801	.5797	.6648	.8252	.9757									
	1.499	.2584	.4347	.5896	.7318	.8654	.9924											
	1.4999	.4592	.7723	1.0472														
0.9	1.0	0.0425	0.0712	0.0958	0.1182	0.1387	0.1575	0.1912	0.2200	0.2497	0.2722	0.2937	0.2732	0.1591				
	1.1	.0456	.0771	.1043	.1288	.1513	.1723	.2101	.2430	.2782	.3069	.3443	.3512	.3170	.2049			
	1.2	.0504	.0857	.1158	.1430	.1684	.1921	.2352	.2737	.3160	.3522	.4074	.4388	.4439	.4176	.3494	.2047	
	1.3	.0572	.0977	.1326	.1642	.1937	.2213	.2722	.3184	.3705	.4170	.4947	.5528	.5916	.6107	.6093	.5863	.5310
	1.4	.0716	.1208	.1638	.2032	.2400	.2748	.3396	.3994	.4682	.5317	.6443	.7404	.8212	.8875	.9401	.9791	1.0053
	1.45	.0876	.1463	.1987	.2466	.2915	.3341	.4138	.4878	.5785	.6591	.8072	.9394	1.0573	1.1628	1.2561	1.3113	1.4097
	1.48	.1105	.1862	.2526	.3136	.3708	.4251	.5272	.6224	.7343	.8396	1.0347						
	1.495	.1571	.2644	.3586	.4451	.5263	.6034	.7487	.8848	1.0452								
	1.499	.2350	.3955	.5361	.6653	.7866	.9034											
	1.4999	.4179	.7026	.9524														

TABLE I - BASIC CALCULATIONS FOR OBTAINING VELOCITY INCREMENT Λ (EQUATION (21)) - Concluded.

[First curvature function, $C/C_a = z^p$.]

$\sqrt{YC_a}$

$M_0 = 0.95$

p	0.02	0.04	0.06	0.08	0.10	0.12	0.16	0.20	0.25	0.30	0.32	0.3218	0.36	0.38	0.384
1.0	0.0353	0.0585	0.0780	0.0948	0.1095	0.1222	0.1418	0.1532	0.1521	0.1153	0.0526	0			
1.1	.0381	.0643	.0852	.1042	.1208	.1367	.1600	.1774	.1881	.1823			0.1281	0.0587	0
1.2	.0422	.0711	.0952	.1168	.1361	.1536	.1838	.2079	.2295	.2407					
1.3	.0479	.0816	.1098	.1352	.1584	.1798	.2178	.2505	.2845	.3106					
1.4	.0593	.1013	.1369	.1691	.1990	.2270	.2783	.3245	.3762	.4218					
1.45	.0738	.1232	.1668	.2066	.2436	.2786	.3434	.4030	.4715	.5340					
1.48	.0934	.1571	.2128	.2639	.3116	.3569	.4415	.5100	.6016	.6972					
1.495	.1328	.2235	.3029	.3758	.4441	.5090	.6310	.7448	.8787	1.0052					
1.499	.1988	.3345	.4533	.5625	.6649	.7622	.9455								
1.4999	.3558	.5939	.8059	1.000											

$M_0 = 0.97$

p	0.02	0.04	0.06	0.08	0.10	0.12	0.16	0.18	0.194	0.1962	0.20	0.22	0.2330	0.25	0.28
1.0	0.0307	0.0501	0.0655	0.0778	0.0872	0.0934	0.0924	0.0782	0.0378	0					
1.1	.0334	.0549	.0723	.0868	.0985	.1076	.1167				0.1068	0.0832	0		
1.2	.0371	.0614	.0814	.0986	.1132	.1256	.1436				.1511			0.1376	0.0979
1.3	.0427	.0709	.0948	.1158	.1344	.1509	.1786				.1992			.2143	
1.4	.0530	.0882	.1192	.1465	.1719	.1952	.2369				.2731			.3114	
1.45	.0645	.1081	.1461	.1805	.2124	.2423	.2972				.3468			.4027	
1.48	.0822	.1382	.1871	.2317	.2733	.3127	.3860				.4534			.5356	
1.495	.1171	.1970	.2669	.3309	.3910	.4479	.5546				.6543			.7610	
1.499	.1754	.2949	.3999	.4959	.5862	.6719	.8331				.9841				
1.4999	.3119	.5244	.7110	.8822	1.0428										

$M_0 = 0.99$

p	0.02	0.04	0.06	0.064	0.0662	0.07	0.0787	0.08	0.09	0.094	0.0993	0.10	0.12	0.13	0.14
1.0	0.0218	0.0316	0.0293	0.0228	0										
1.1	.0240	.0363	.0403			0.0366	0								
1.2	.0271	.0422	.0511					0.0519	0.0450	0.0402	0				
1.3	.0315	.0505	.0644					.0737				0.0775	0.0725	0.0627	0.0246
1.4	.0397	.0652	.0860					.1035				.1182	.1300		
1.45	.0487	.0809	.1082					.1324				.1540	.1736		
1.48	.0624	.1044	.1407					.1736				.2038	.2321		
1.495	.0891	.1496	.2024					.2507				.2958	.3383		
1.499	.1335	.2244	.3037					.3771				.4455	.5104		
1.4999	.2376	.3994	.5414					.6714				.7939	.9101		

$\sqrt{YC_a}$

$M_0 = 0.95$

p	0.40	0.484	0.485	0.50	0.60	0.67	0.679	0.70	0.80	0.90	1.0
1.0											
1.1											
1.2	0.2191	0.0293	0								
1.3	.3396			0.3303	0.2625	0.1265	0				
1.4	.4966			.5509	.5846			0.5978	0.5897	0.5597	0.5059
1.45	.6447			.7383	.8160			.8792	.9289	.9658	
1.48	.8535			.9932							
1.495											
1.499											
1.4999											

$M_0 = 0.97$

p	0.2943	0.30	0.40	0.4169	0.50	0.60	0.70	0.75	0.7848	0.80	0.90	1.0
1.0												
1.1												
1.2	0											
1.3		0.2149	0.1168	0								
1.4		.3423	.3826		0.3911	0.3608	0.2718	0.1817	0			
1.45		.3525	.5361		.6000	.6453	.6723			0.6815	0.6729	0.6469
1.48		.6038	.7336		.8466	.9296						
1.495		.8809	1.0841									
1.499												
1.4999												

$M_0 = 0.99$

p	0.1407	0.16	0.20	0.25	0.26	0.2649	0.30	0.40	0.50	0.5133	0.60	0.70	0.80	0.90	1.0
1.0															
1.1															
1.2															
1.3	0														
1.4		0.1452	0.1457	0.0998	0.0644	0									
1.45		.2073	.2342	.2650			0.2793	0.2576	0.1114	0					
1.48		.2837	.3297	.3809			.4257	.4979	.5484		0.5778	0.5859	0.5726	0.5367	0.4689
1.495		.4177	.4911	.5764			.6554	.7986	.9250						
1.499		.6323	.7461	.8797			1.0057								
1.4999															
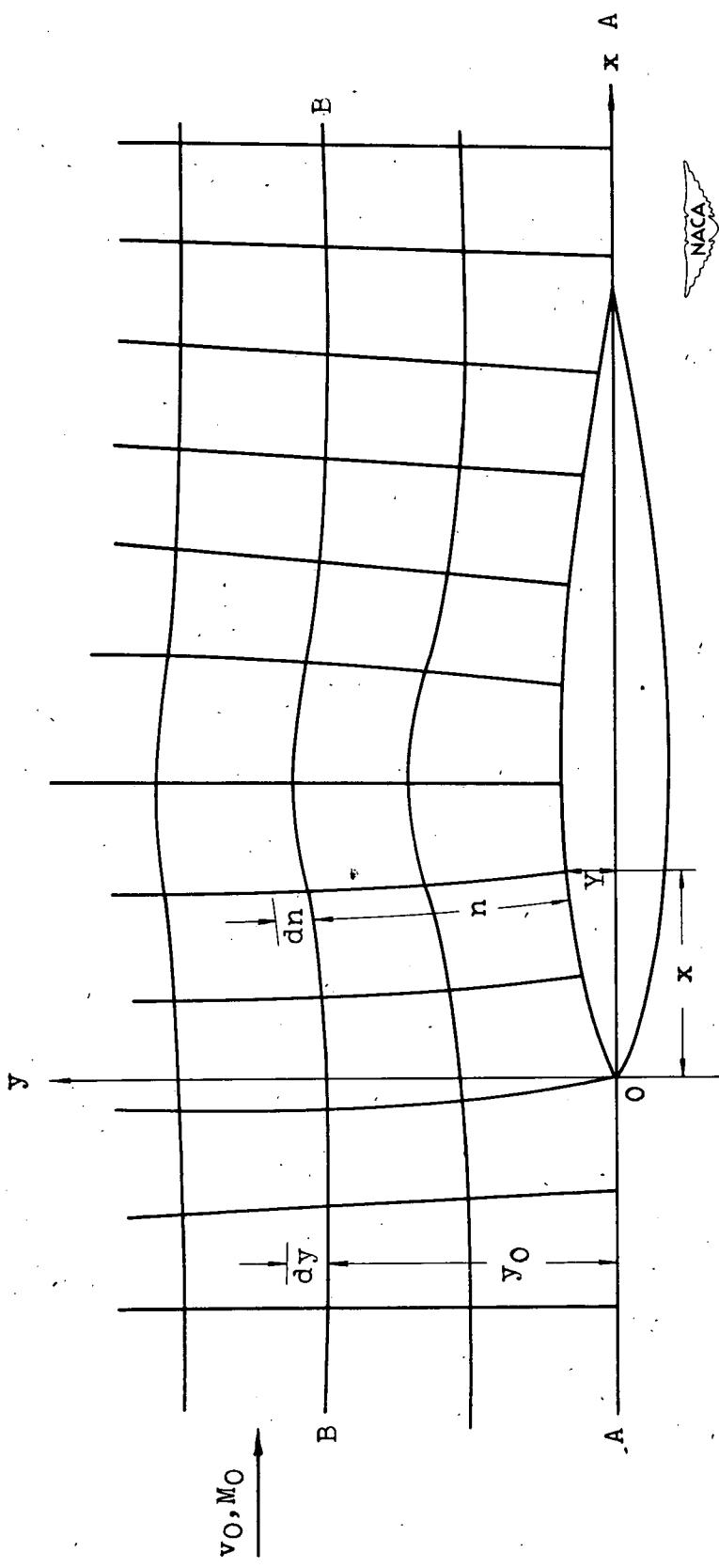
Figure 1. — Meridian section of body of revolution in axially symmetric compressible flow.

(a) Free-stream Mach number M_0, 0.
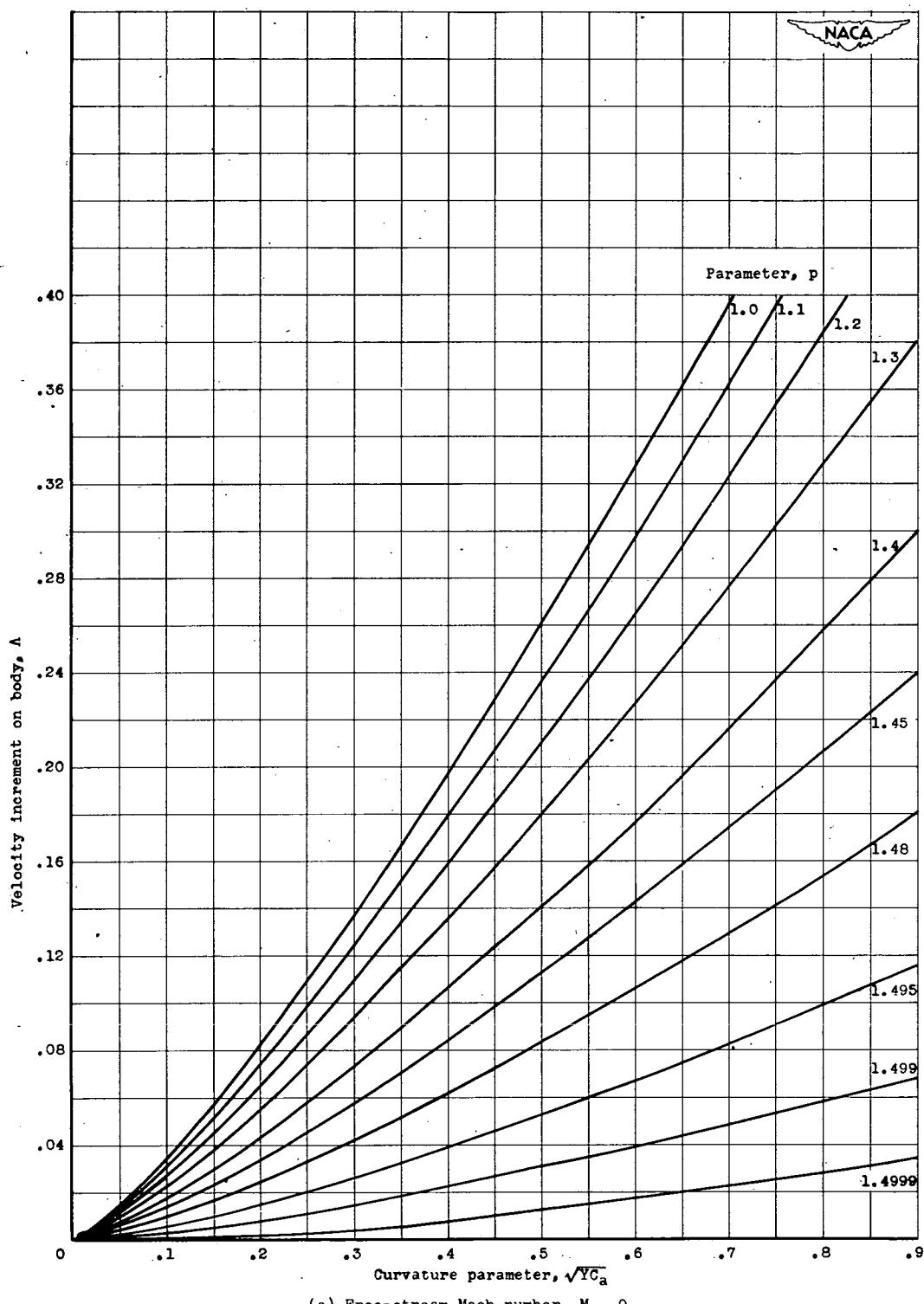
Figure 2. - Velocity increment on surface of body of revolution as function of curvature parameter of body $\sqrt{YC_a}$ for several values of parameter p. Values computed from equation (21) and tabulated in table I.

(b) Free-stream Mach number M_0, 0.4.
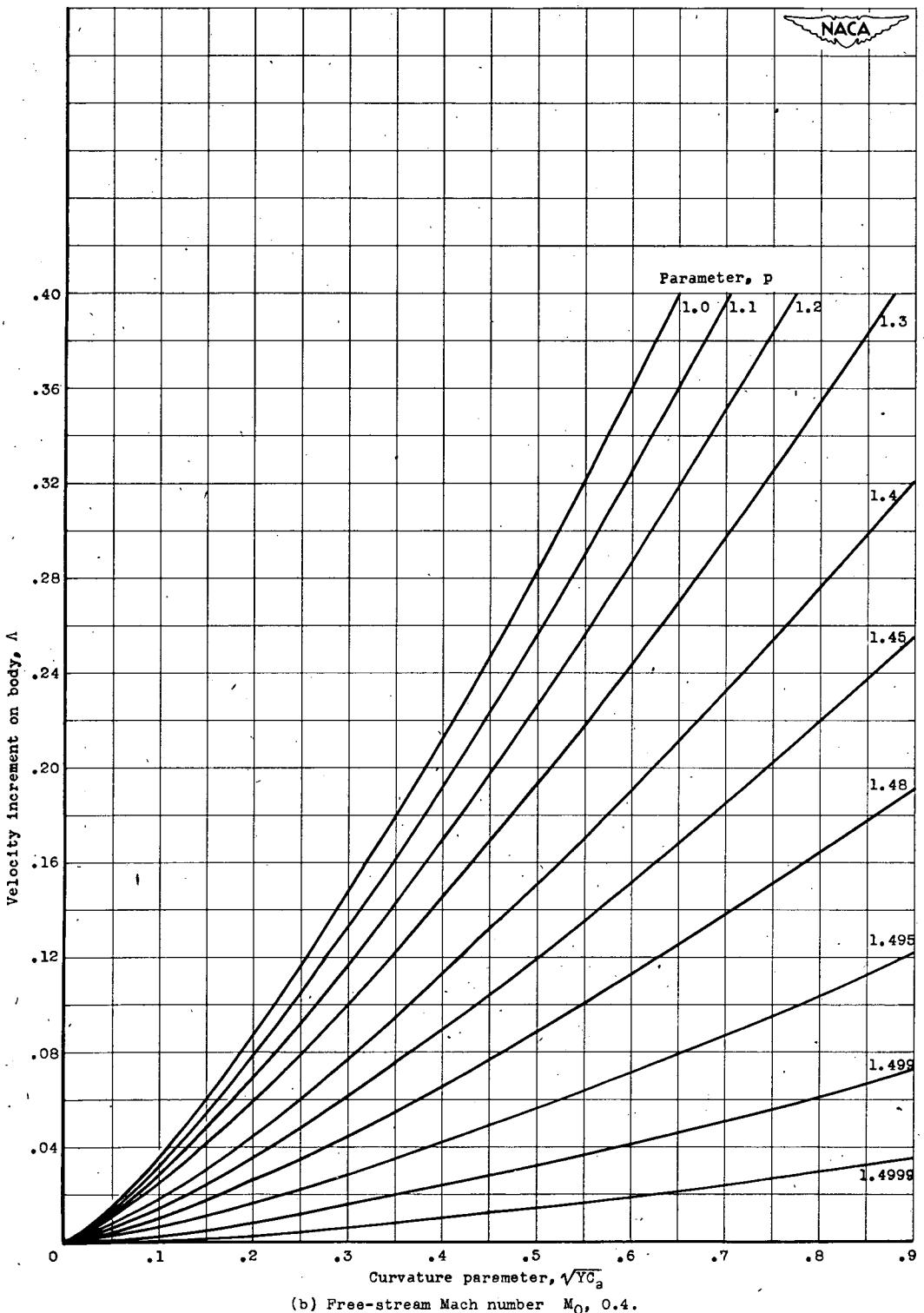
Figure 2. - Continued. Velocity increment on surface of body of revolution as function of curvature parameter of body $\sqrt{YC_a}$ for several values of parameter p. Values computed from equation (21) and tabulated in table I.
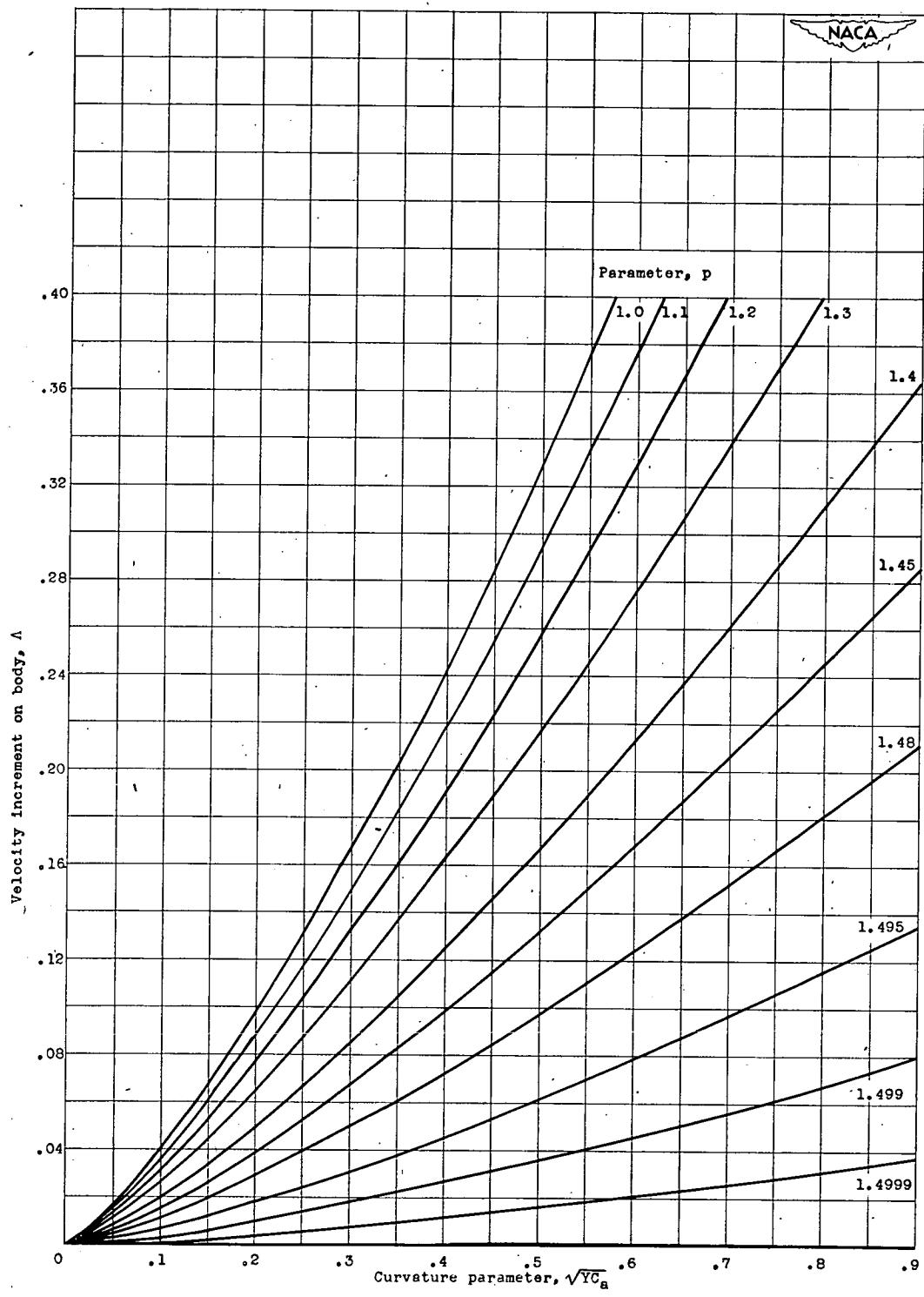
(c) Free-stream Mach number M_0, 0.6.

Figure 2. - Continued. Velocity increment on surface of body of revolution as function of curvature parameter of body $\sqrt{YC_a}$ for several values of parameter p. Values computed from equation (21) and tabulated in table I.
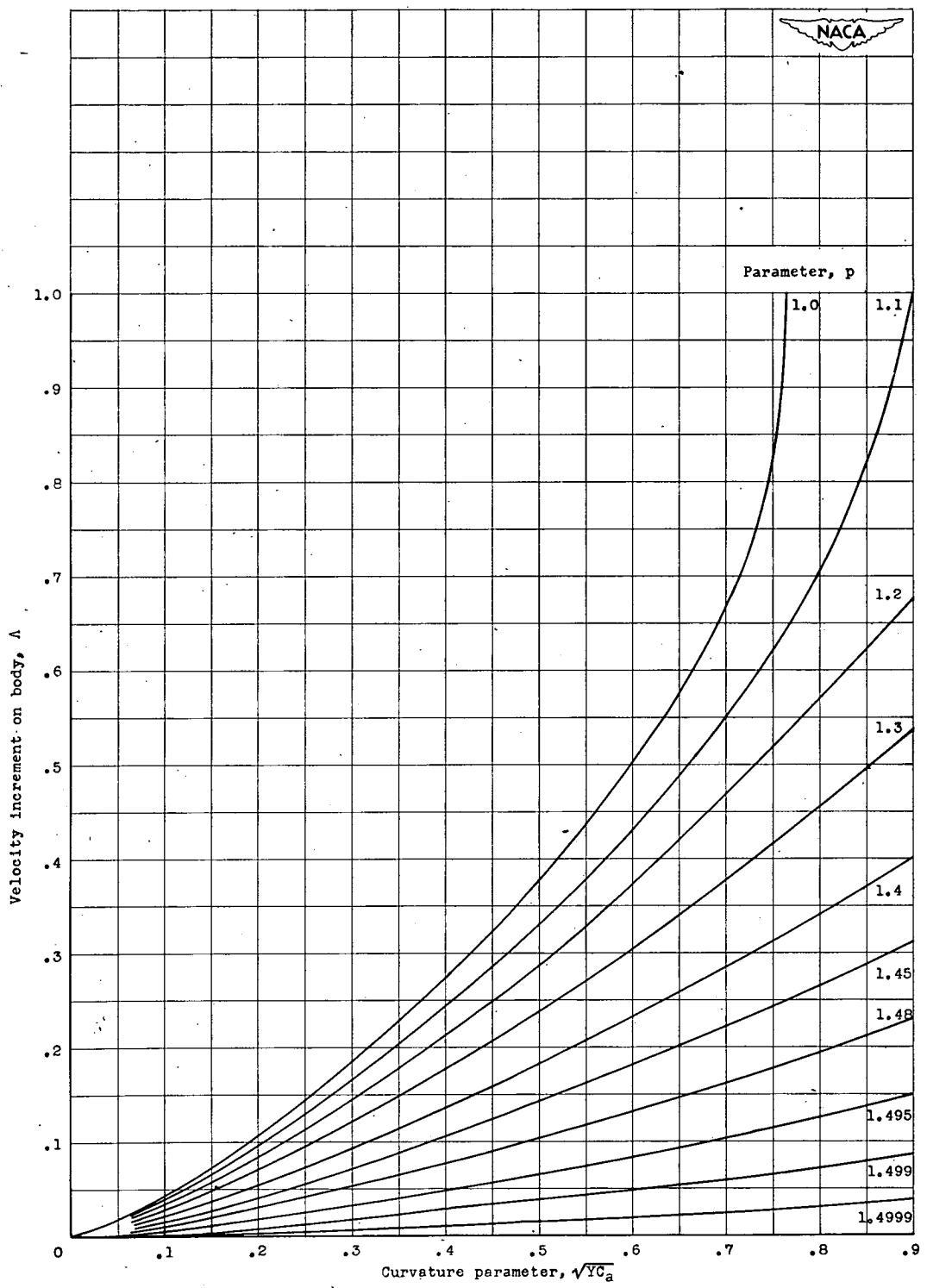
(d) Free stream Mach number M_0, 0.7.

Figure 2. - Continued. Velocity increment on surface of body of revolution as function of curvature parameter of body $\sqrt{YC_a}$ for several values of parameter p. Values computed from equation (21) and tabulated in table I.
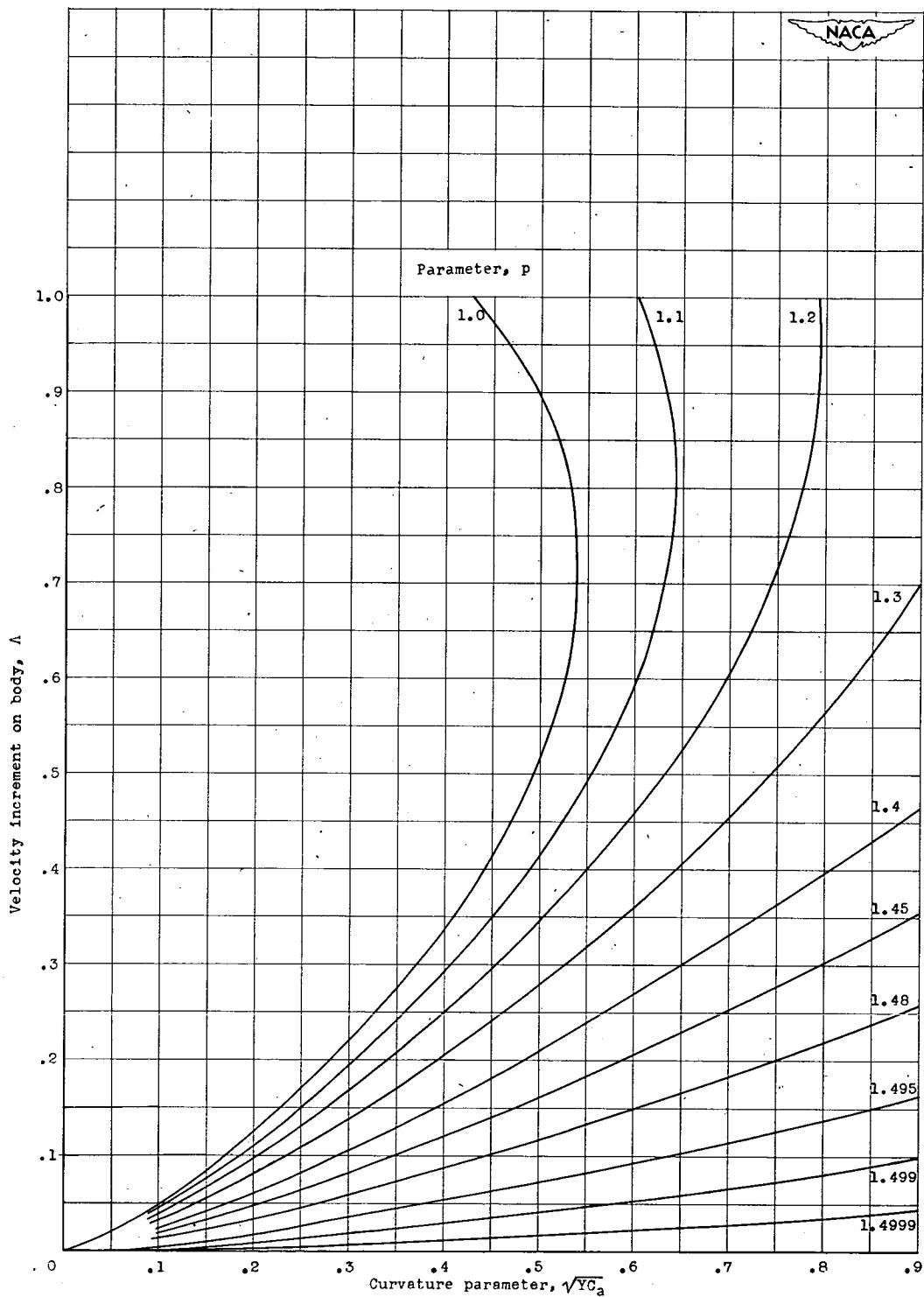
(e) Free-stream Mach number M_0, 0.8.

Figure 2. - Continued. Velocity increment on surface of body of revolution as function of
curvature parameter of body $\sqrt{YC_a}$ for several values of parameter p. Values computed
from equation (21) and tabulated in table I.
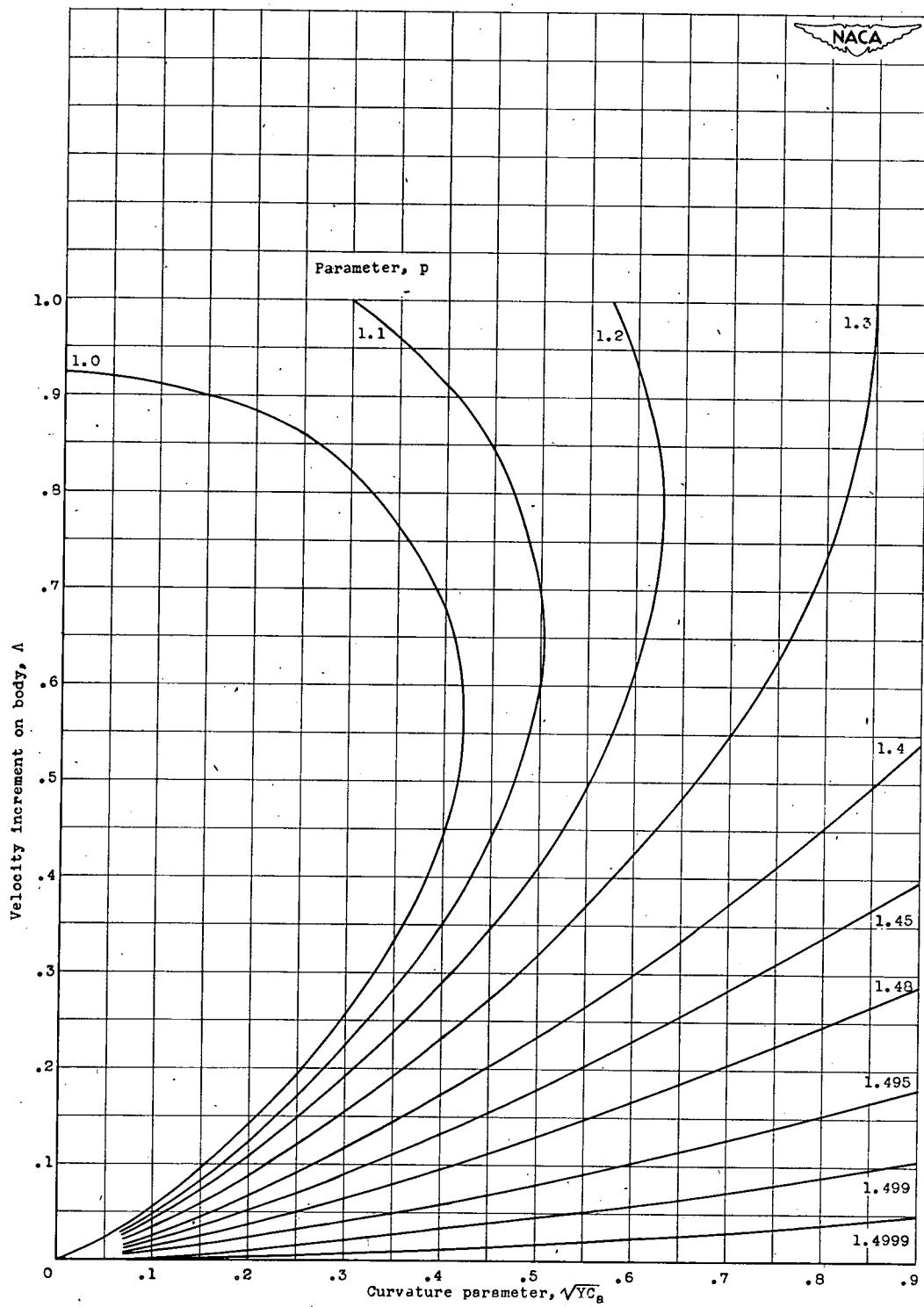
(f) Free-stream Mach number M_0, 0.85.

Figure 2. - Continued. Velocity increment on surface of body of revolution as function of curvature parameter of body $\sqrt{YC_a}$ for several values of parameter p. Values computed from equation (21) and tabulated in table I.
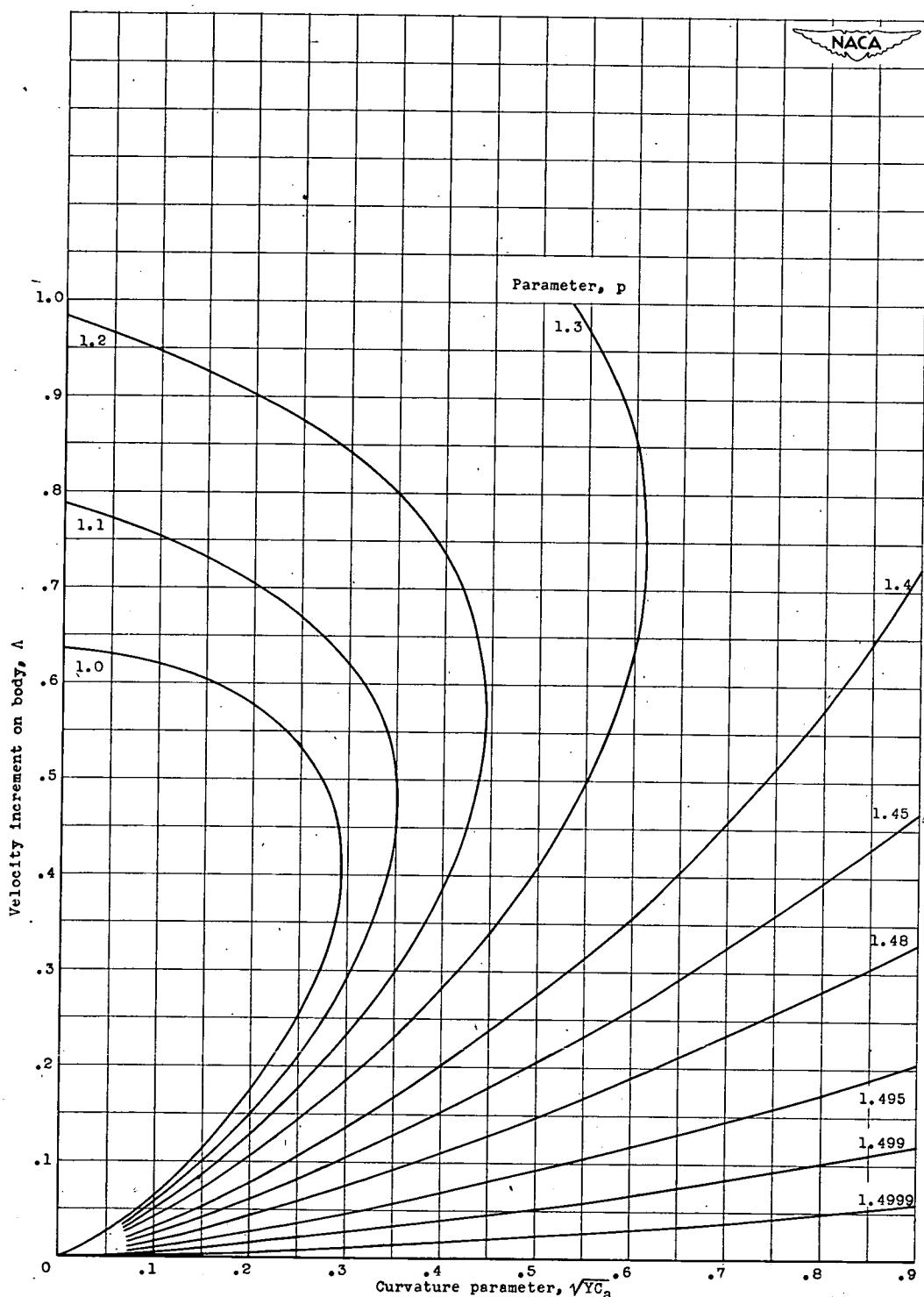
(g) Free-stream Mach number M_0, 0.90.

Figure 2. - Continued. Velocity increment on surface of body of revolution as function of
curvature parameter of body $\sqrt{YC_a}$ for several values of parameter p. Values computed
from equation (21) and tabulated in table I.
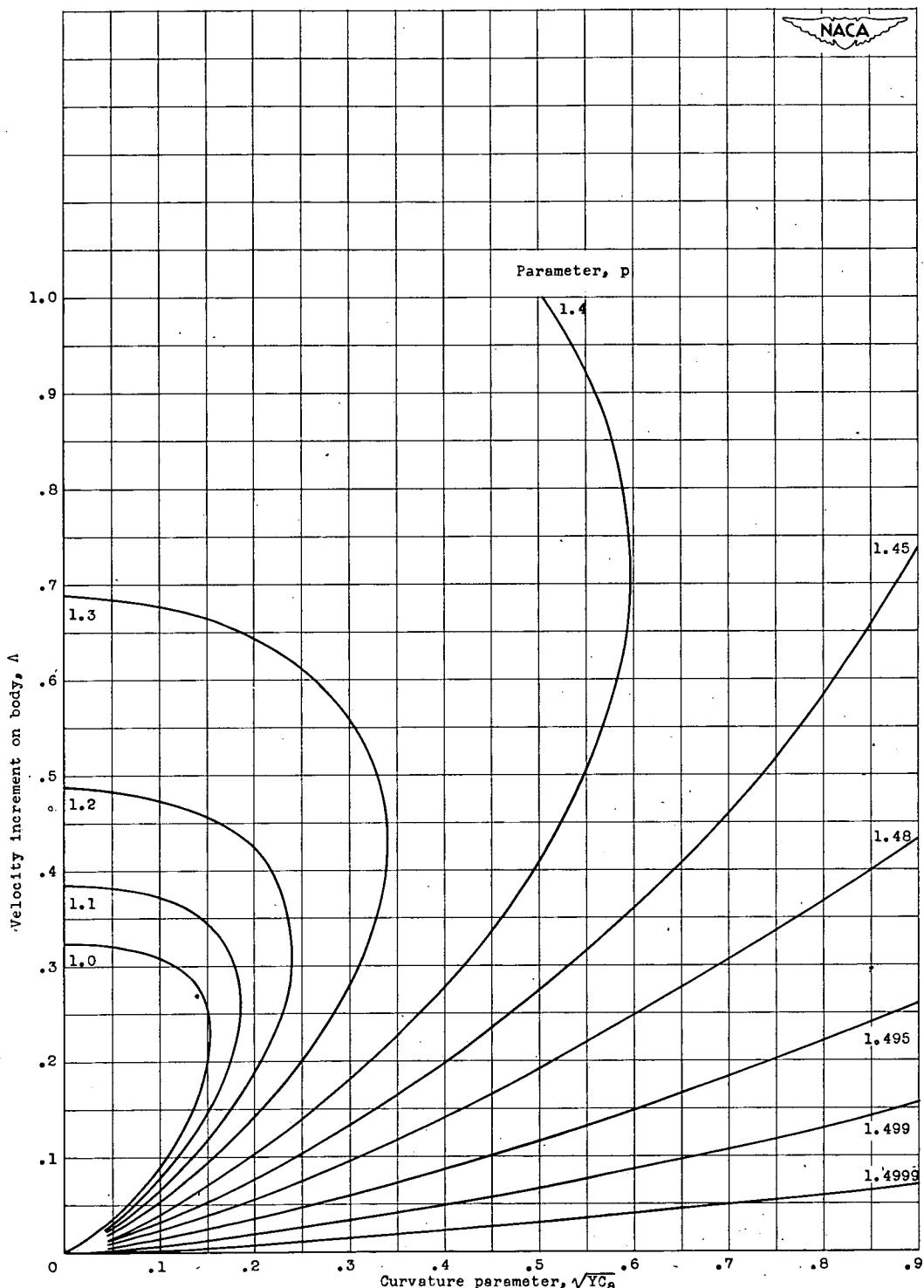
(h) Free-stream Mach number M_0, 0.95.

Figure 2. - Continued. Velocity increment on surface of body of revolution as function of curvature parameter of body $\sqrt{YC_a}$ for several values of parameter p. Values computed from equation (21) and tabulated in table I.
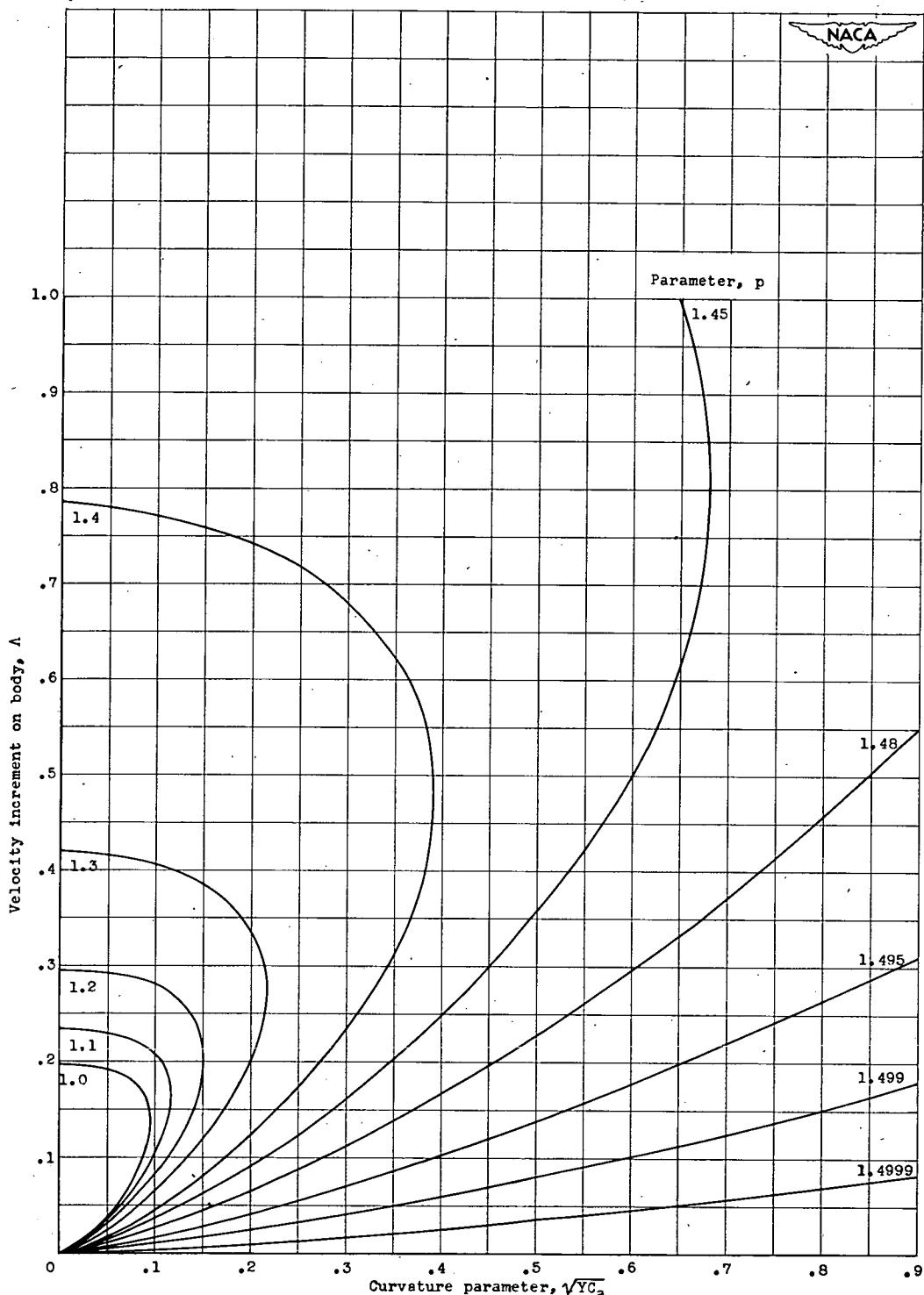
(i) Free-stream Mach number M_0, 0.97.

Figure 2. - Continued. Velocity increment on surface of body of revolution as function of
curvature parameter of body $\sqrt{YC_a}$ for several values of parameter p. Values computed
from equation (21) and tabulated in table I.
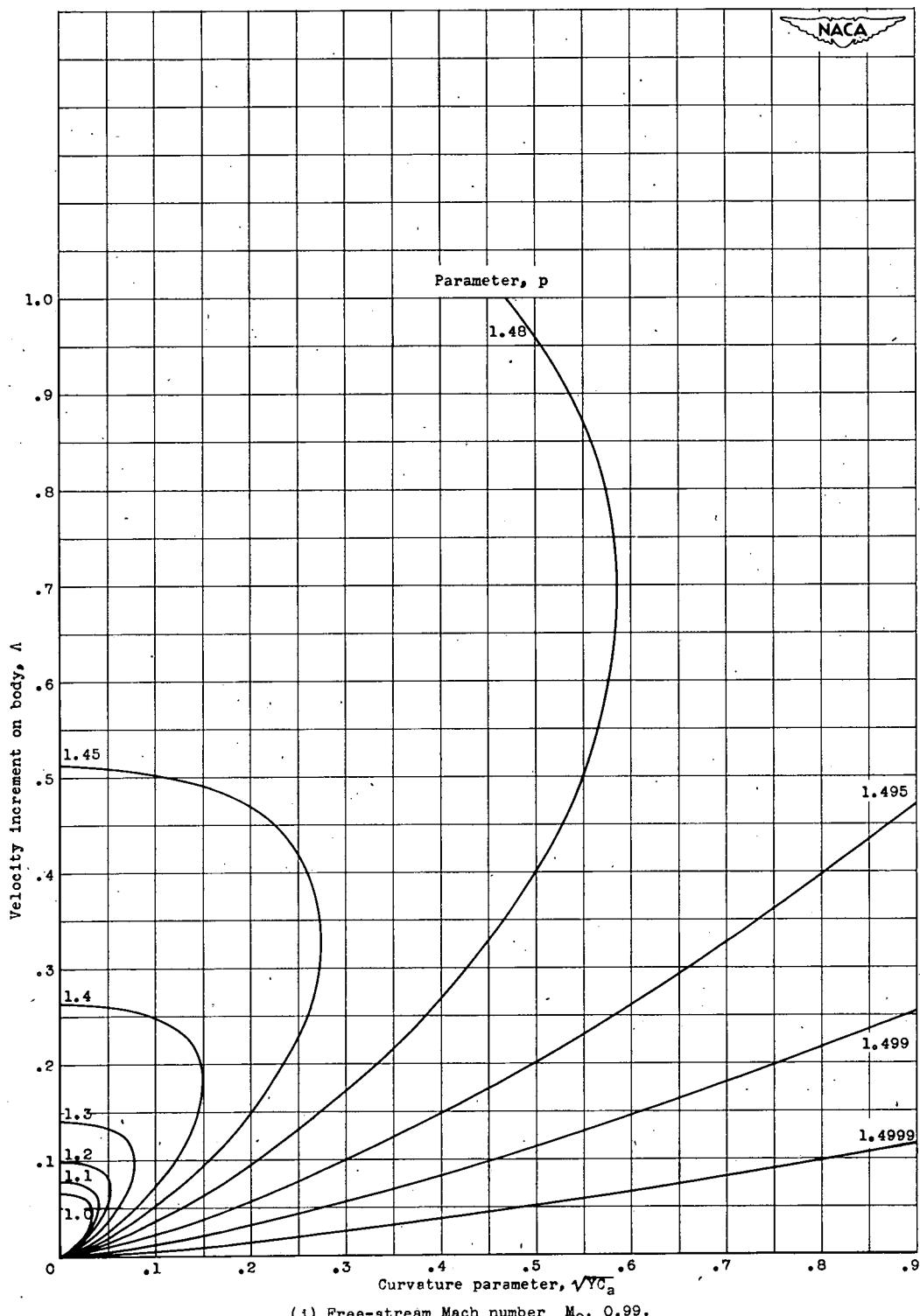
(j) Free-stream Mach number M_0, 0.99.

Figure 2. - Concluded. Velocity increment on surface of body of revolution as function of
curvature parameter of body $\sqrt{YC_a}$ for several values of parameter p. Values computed
from equation (21) and tabulated in table I.

$$\chi = \frac{YC_a}{2} \frac{\Gamma_c^2}{\mu^3} \frac{(2-q)^3}{(3-q)^2}$$
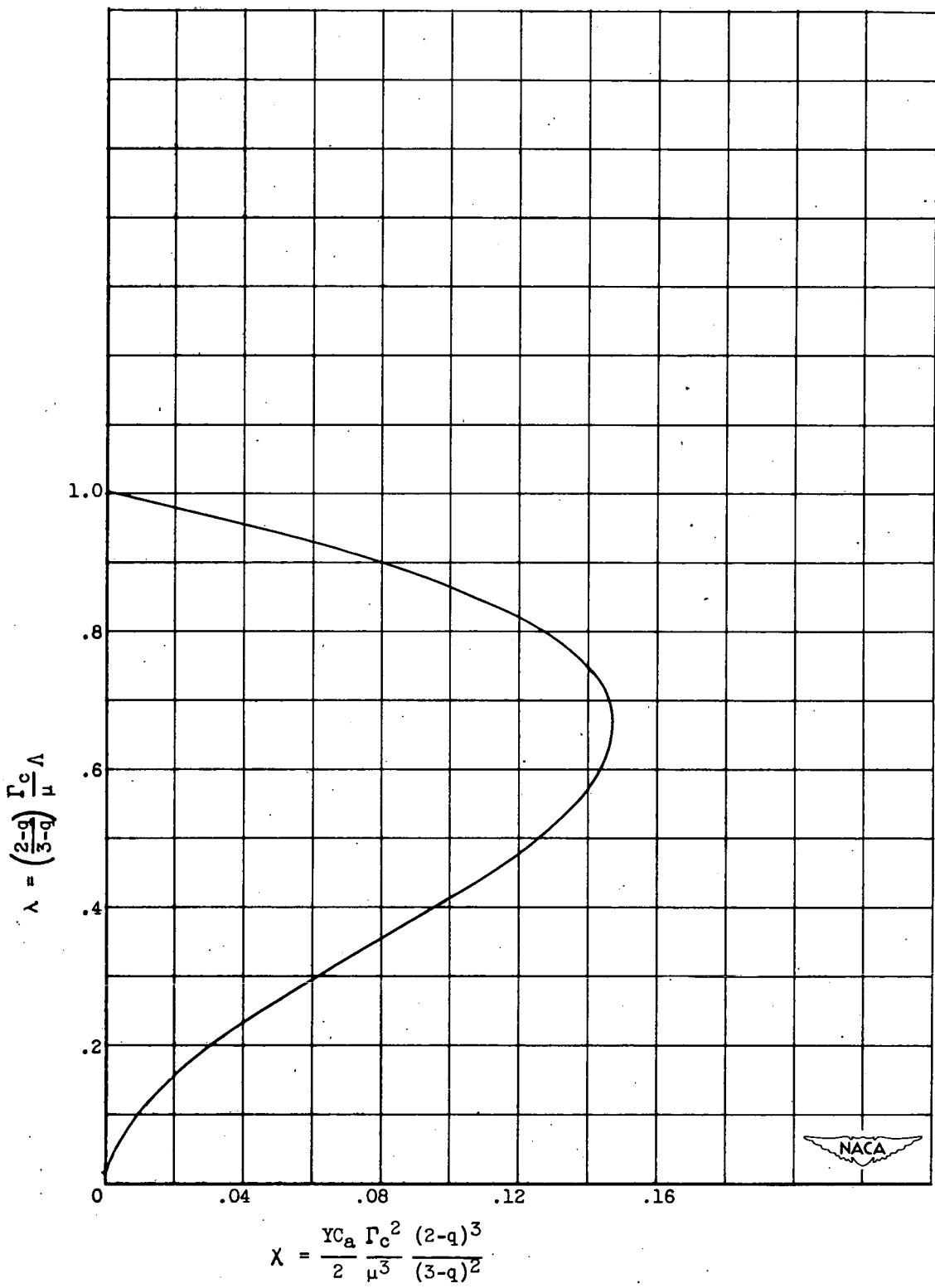
Figure 3. - Plot of equation (35); $\chi = \lambda^2 - \lambda^3$.
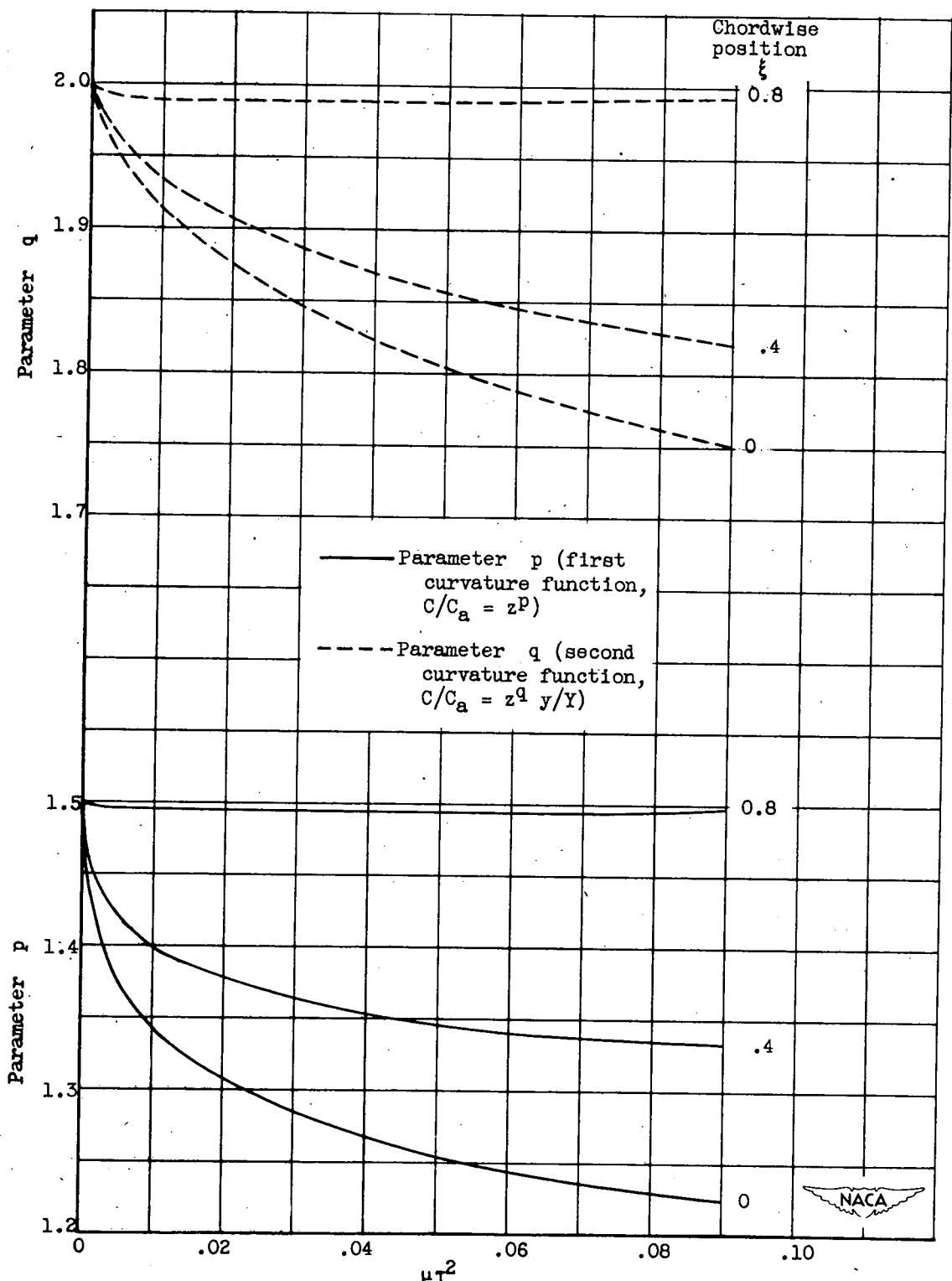
Figure 4. - Curvature-function parameters p and q as functions of $\mu_T{}^2$ for several chordwise positions on ellipsoid of revolution.
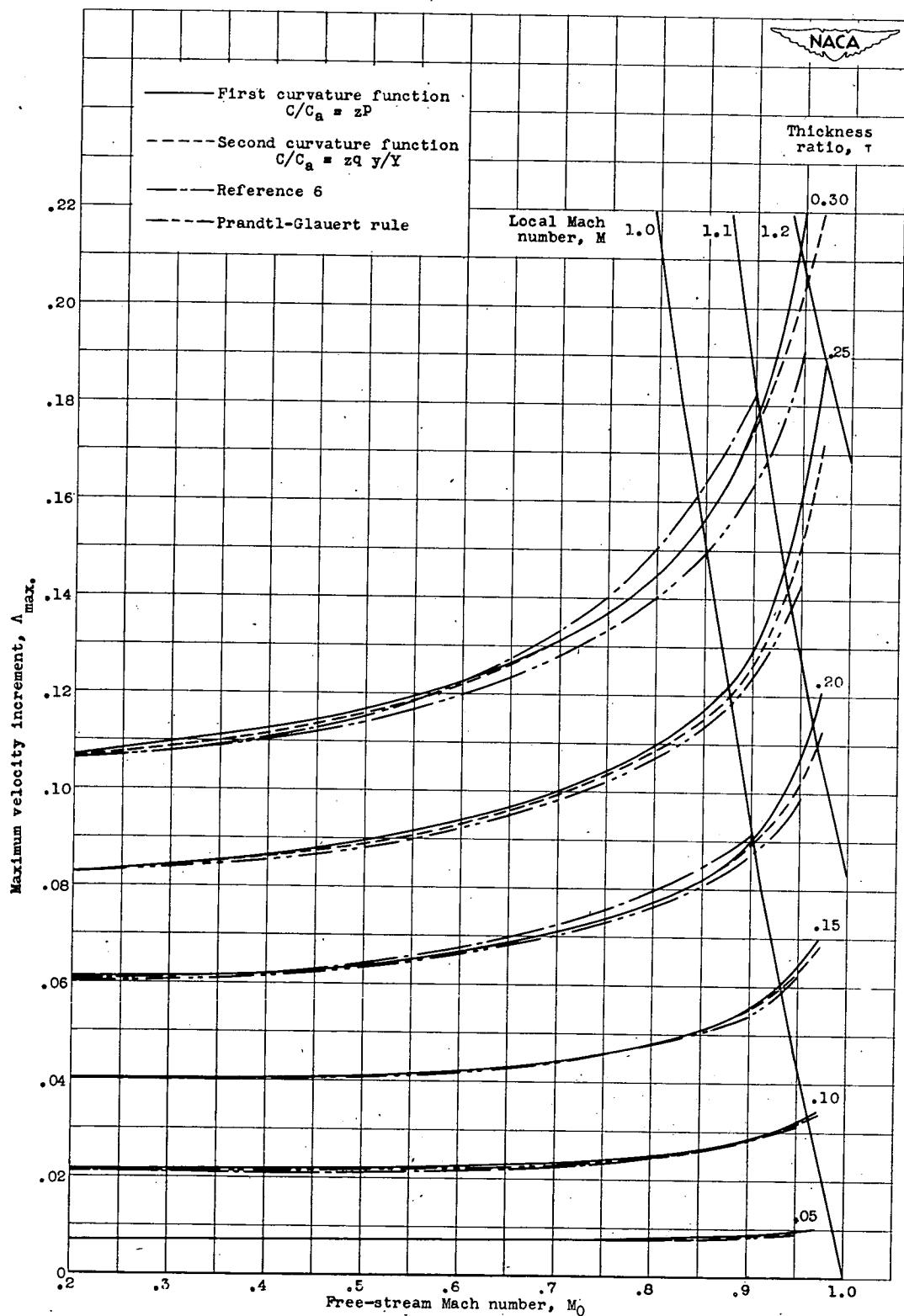
Figure 5. – Variation of maximum velocity increment at midchord of ellipsoid of
revolution as function of free–stream Mach number for several thickness ratios.
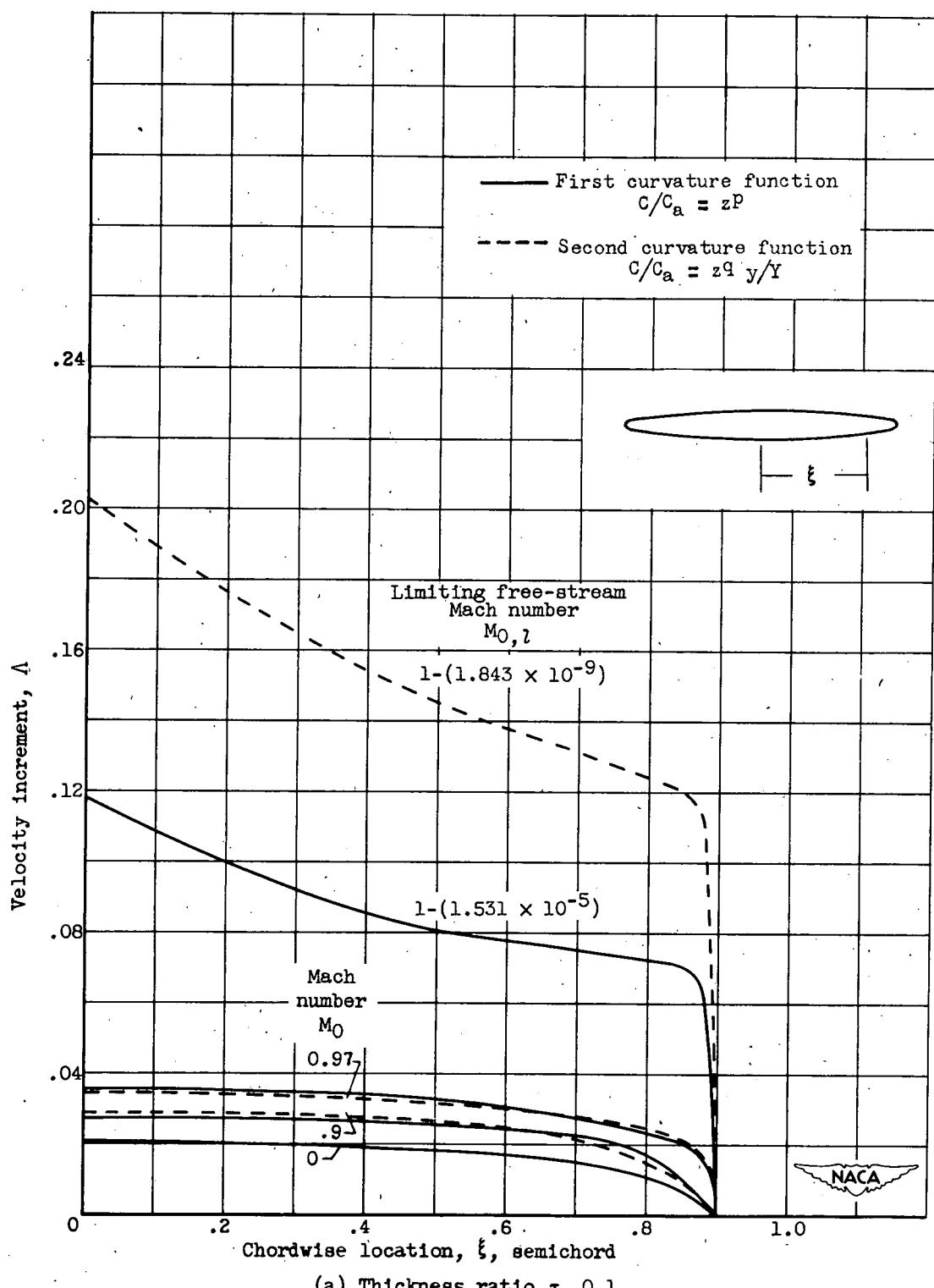
(a) Thickness ratio τ, 0.1.

Figure 6. - Velocity distribution on ellipsoid of revolution for several
Mach numbers.

(b) Thickness ratio τ, 0.3.
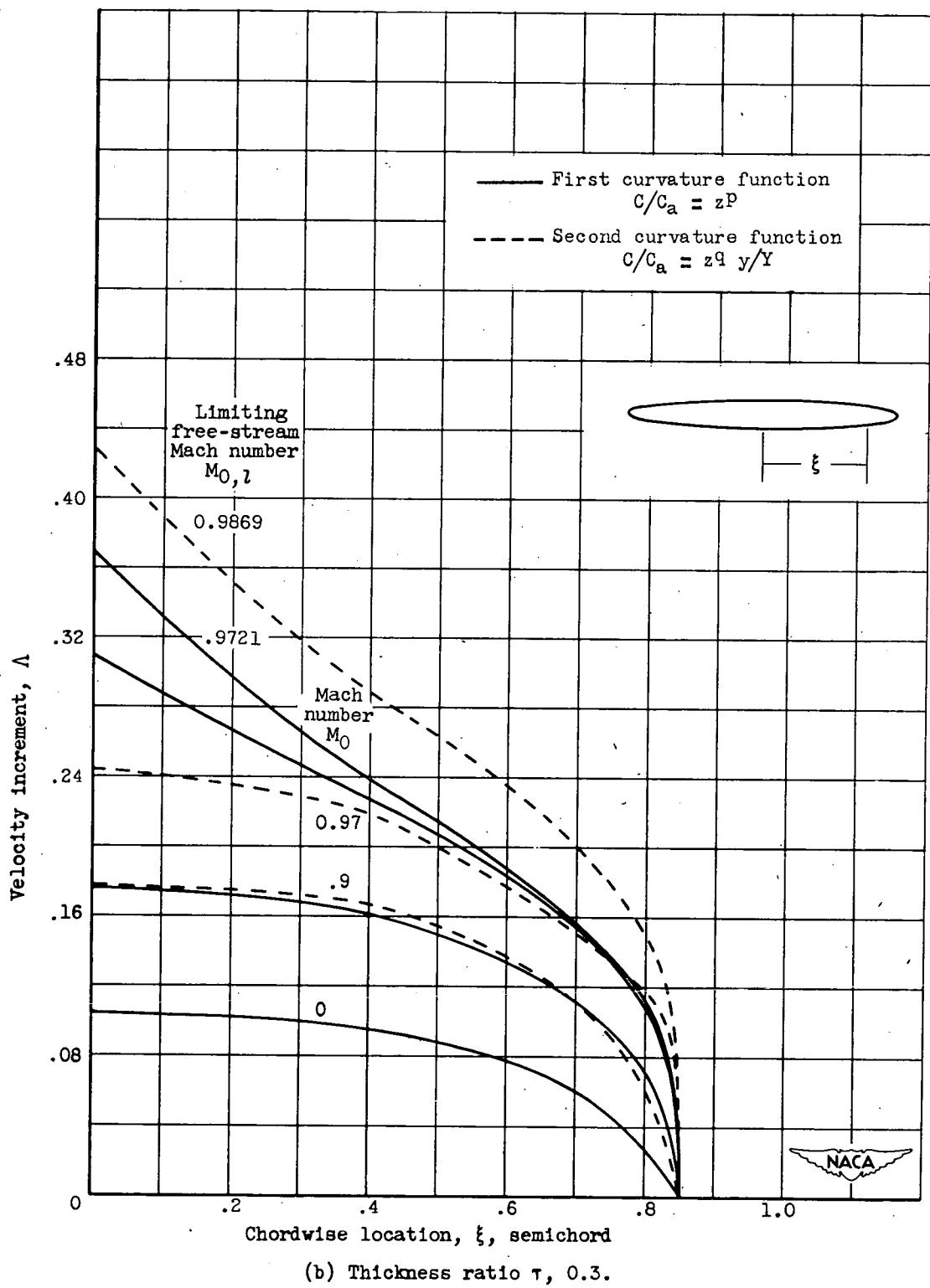
Figure 6. - Concluded. Velocity distribution on ellipsoid of revolution for several Mach numbers.
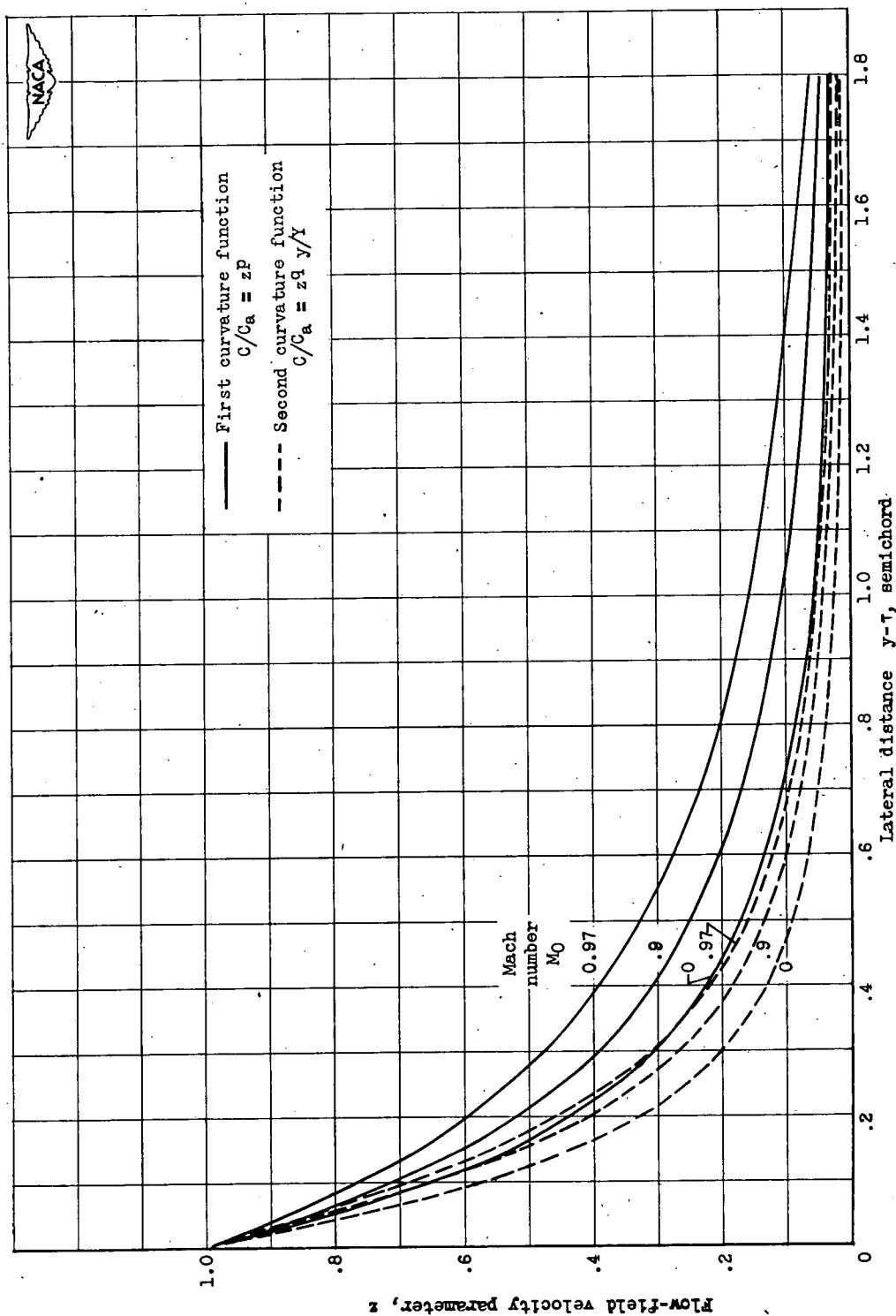
Figure 7. - Lateral variation of velocity in flow field of ellipsoid of revolution at midchord location for several Mach numbers.

(a) Thickness ratio τ, 0.1.
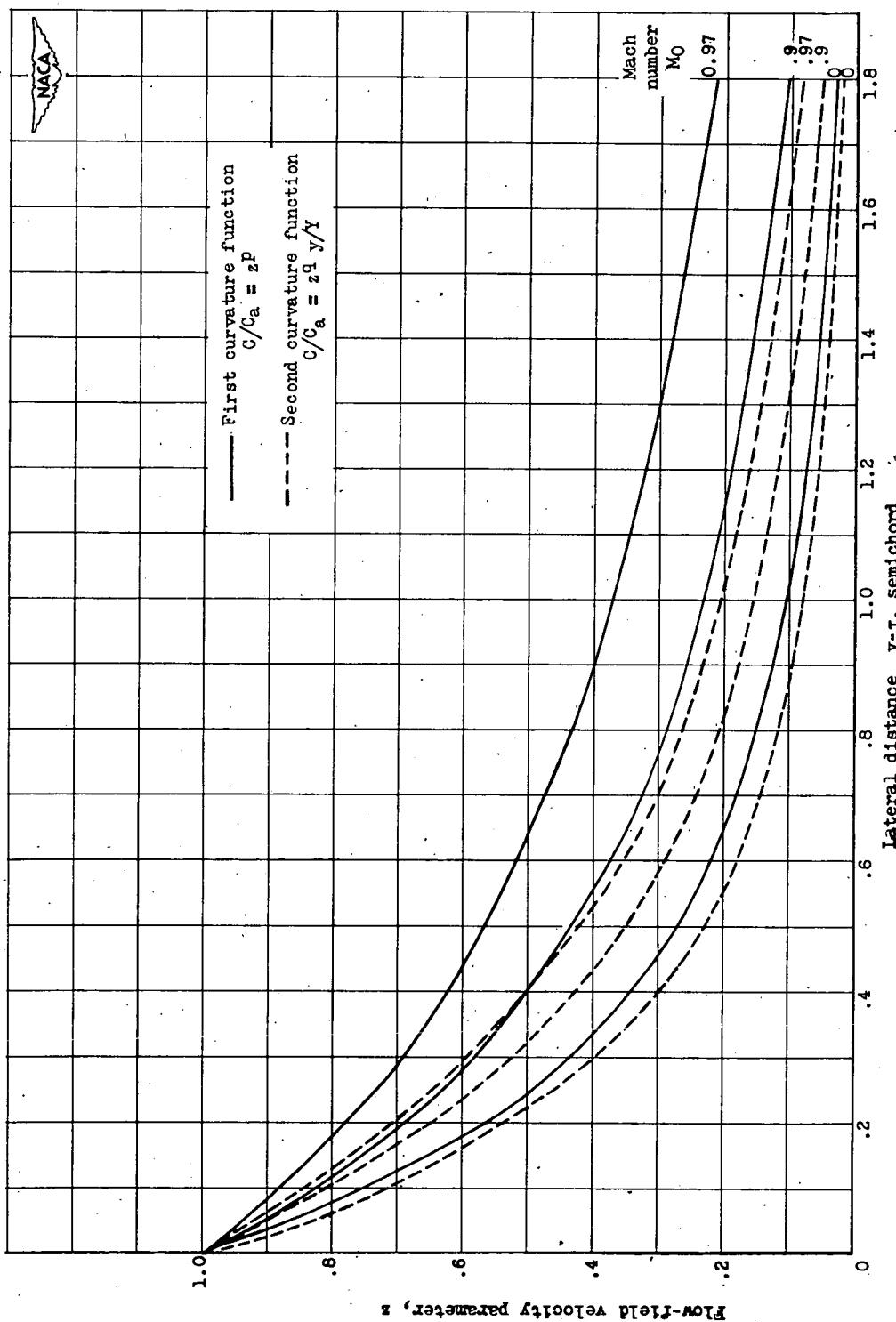
Figure 7. - Concluded. Lateral variation of velocity in flow field of ellipsoid of revolution at midchord location for several Mach numbers.

(b) Thickness ratio τ, 0.3.
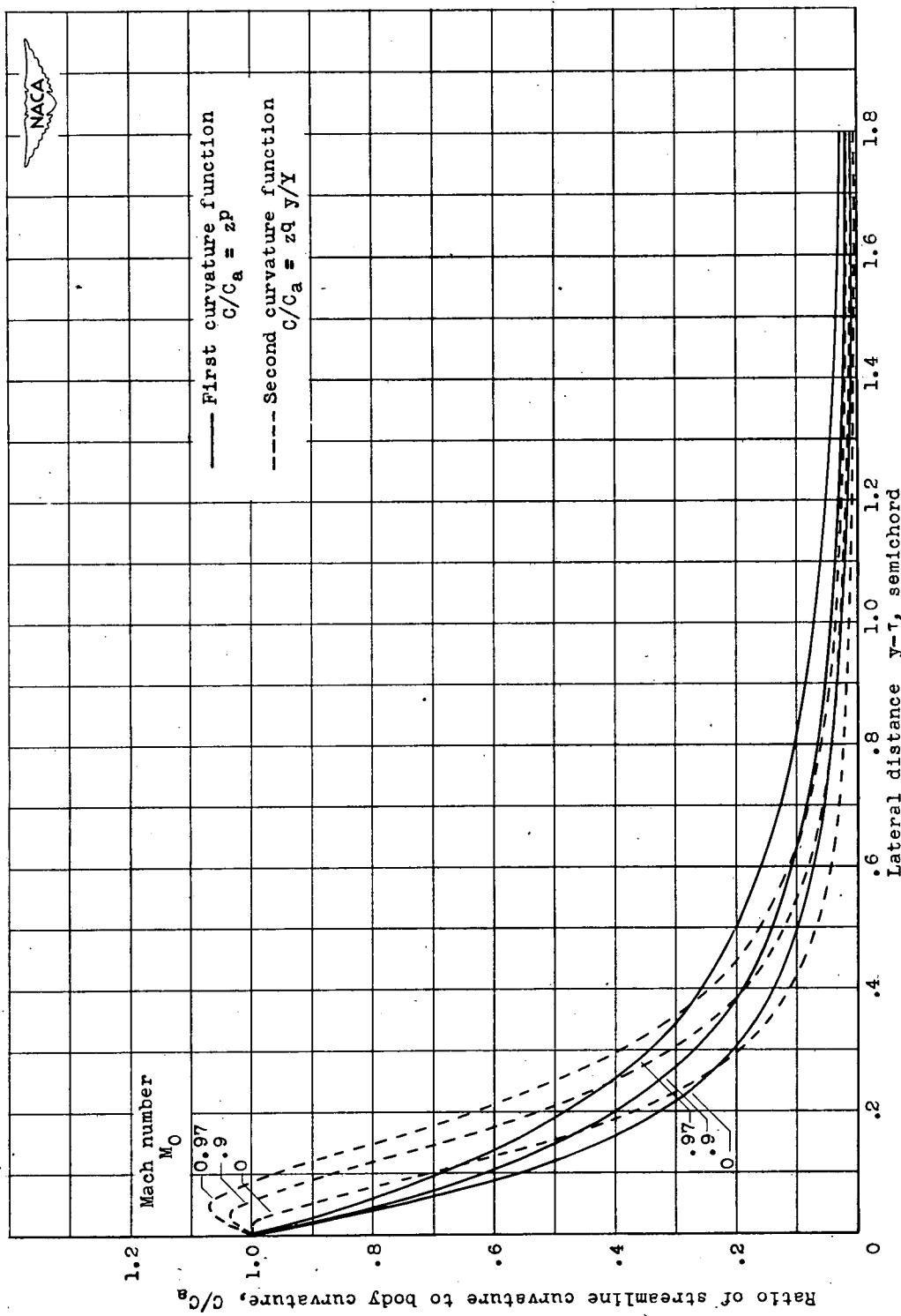
Figure 8. — Lateral variation of streamline curvature in flow field of ellipsoid of revolution at midchord location for several Mach numbers.

(a) Thickness ratio τ, 0.1.
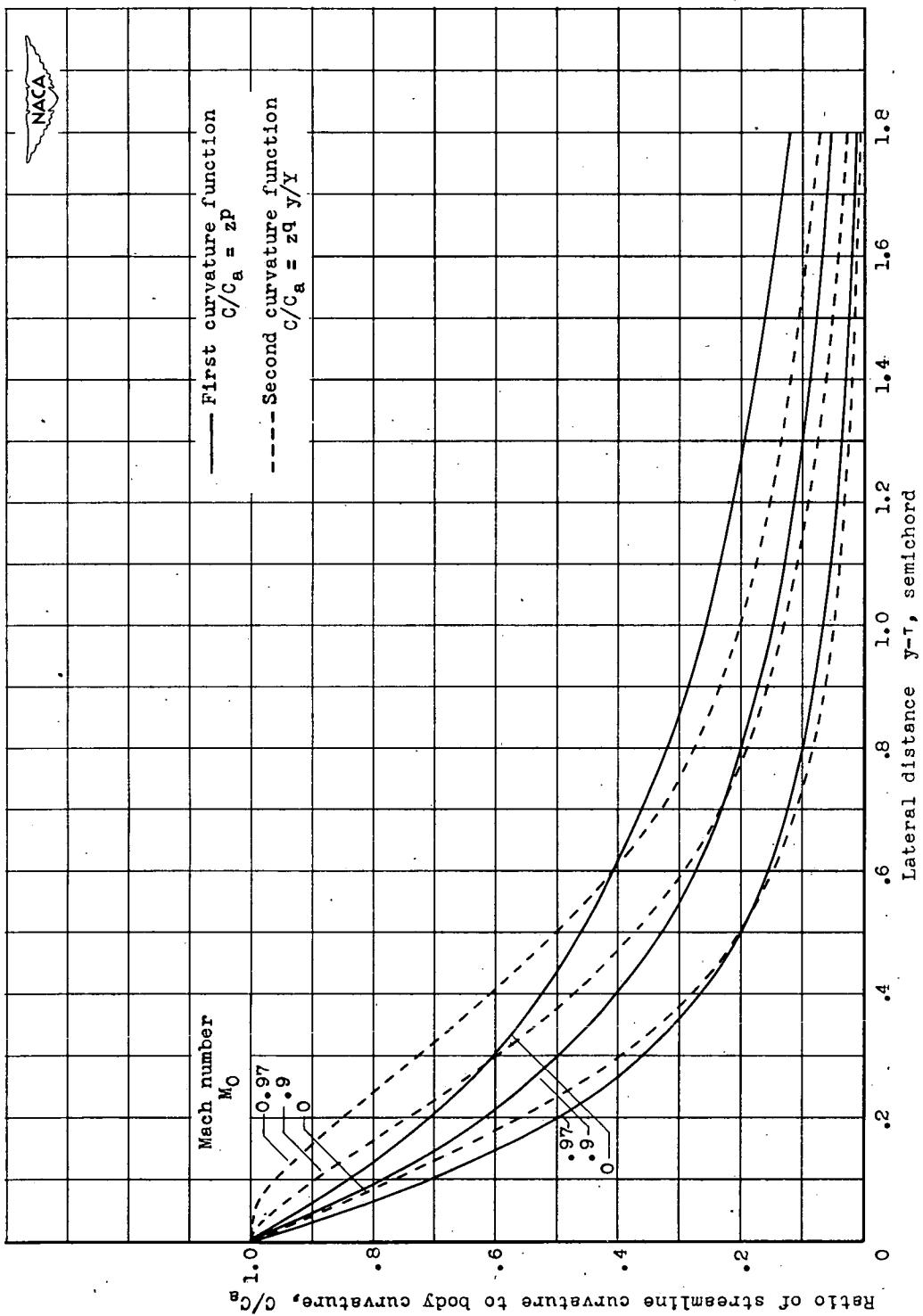
Figure 8. - Concluded. Lateral variation of streamline curvature in flow field of ellipsoid of revolution at midchord location for several Mach numbers.

(a) Thickness ratio τ, 0.1.
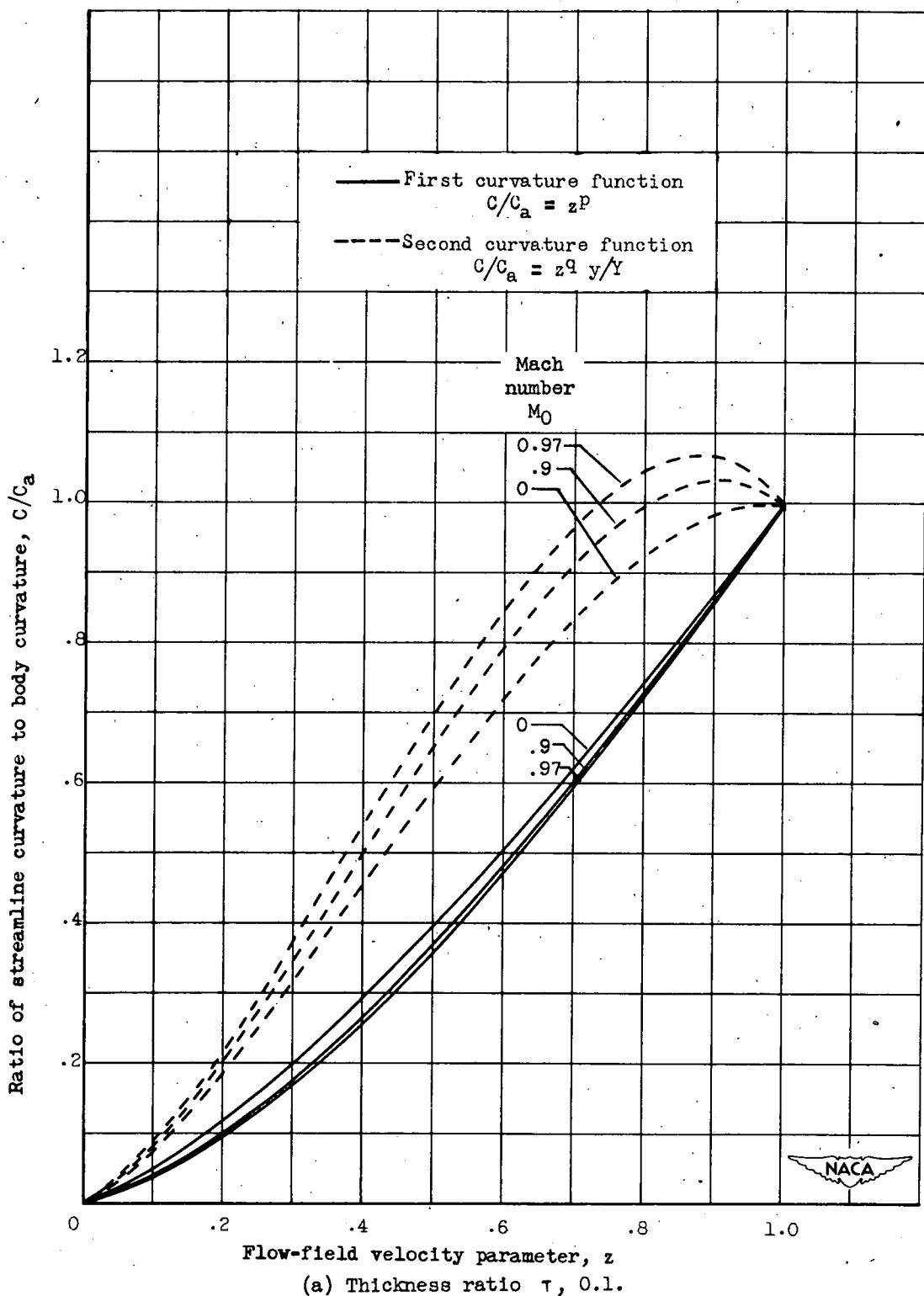
Figure 9. - Variation of streamline curvature with velocity in flow field of ellipsoid of revolution for several Mach numbers.

(b) Thickness ratio τ, 0.3.
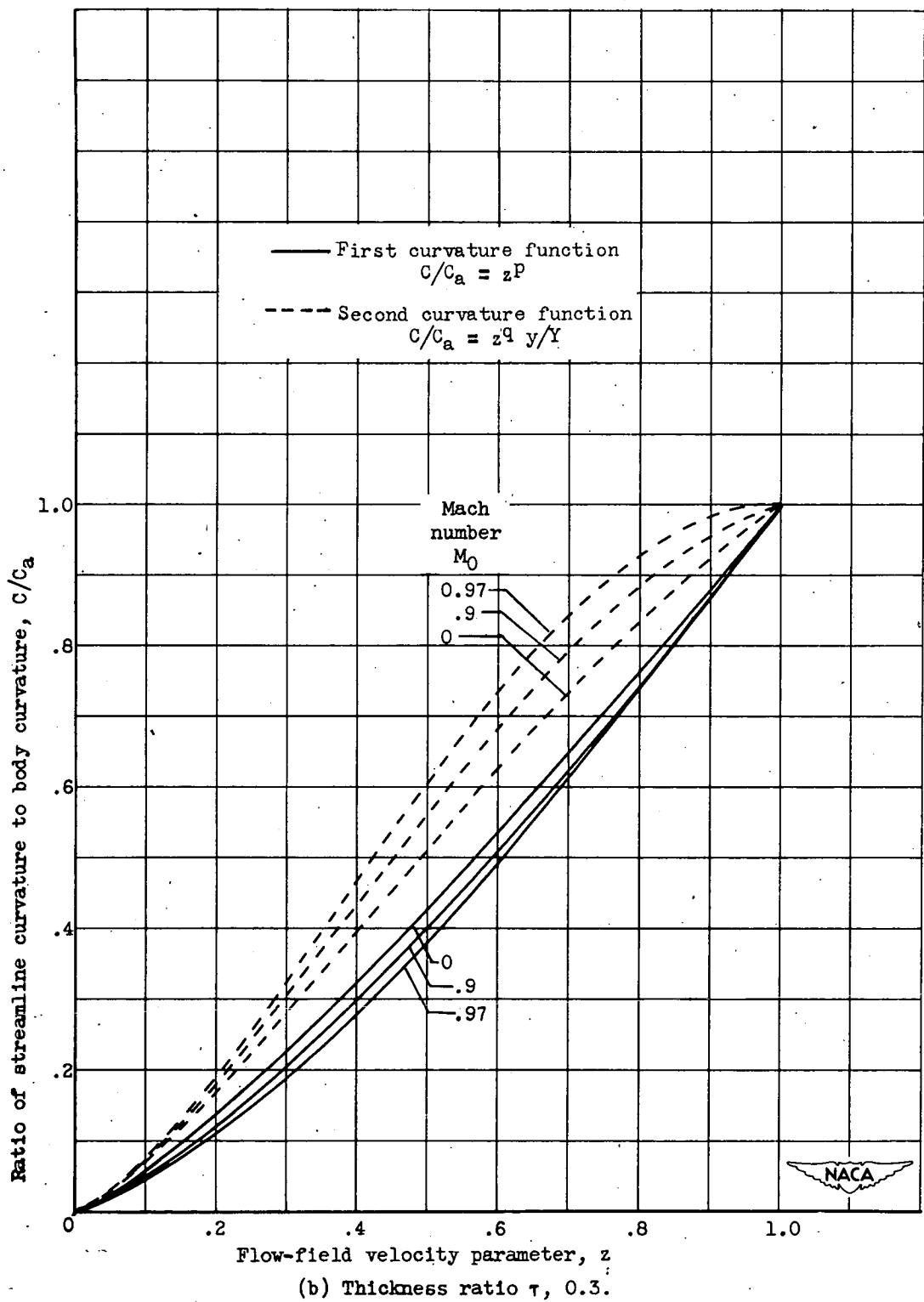
Figure 9. - Concluded. Variation of streamline curvature with velocity in
flow field of ellipsoid of revolution for several Mach numbers.
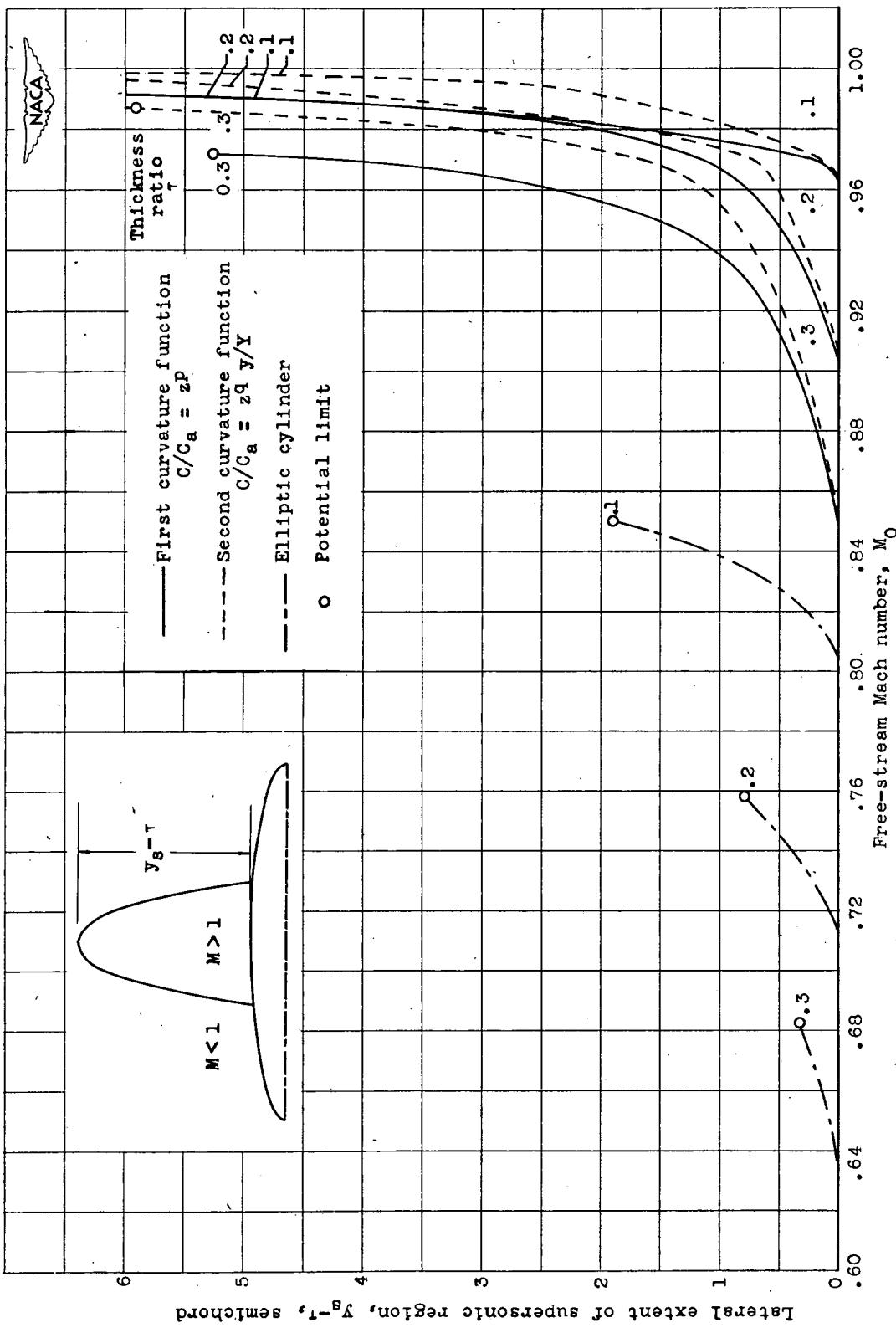
Figure 10. - Lateral extent of supersonic region at midchord location for ellipsoid of revolution and elliptic cylinder.
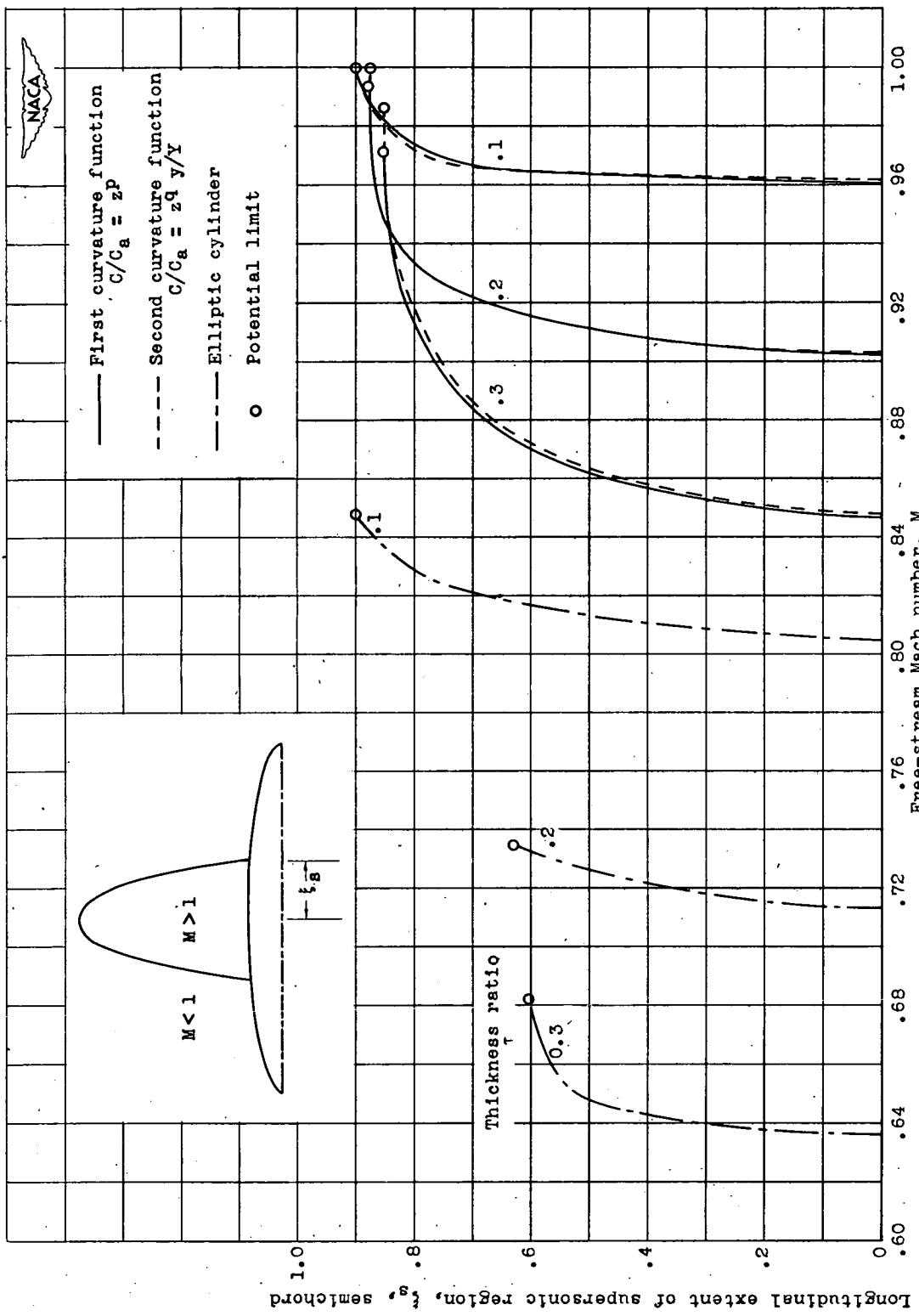
Figure 11. – Longitudinal extent of supersonic region for ellipsoid of revolution and elliptic cylinder.
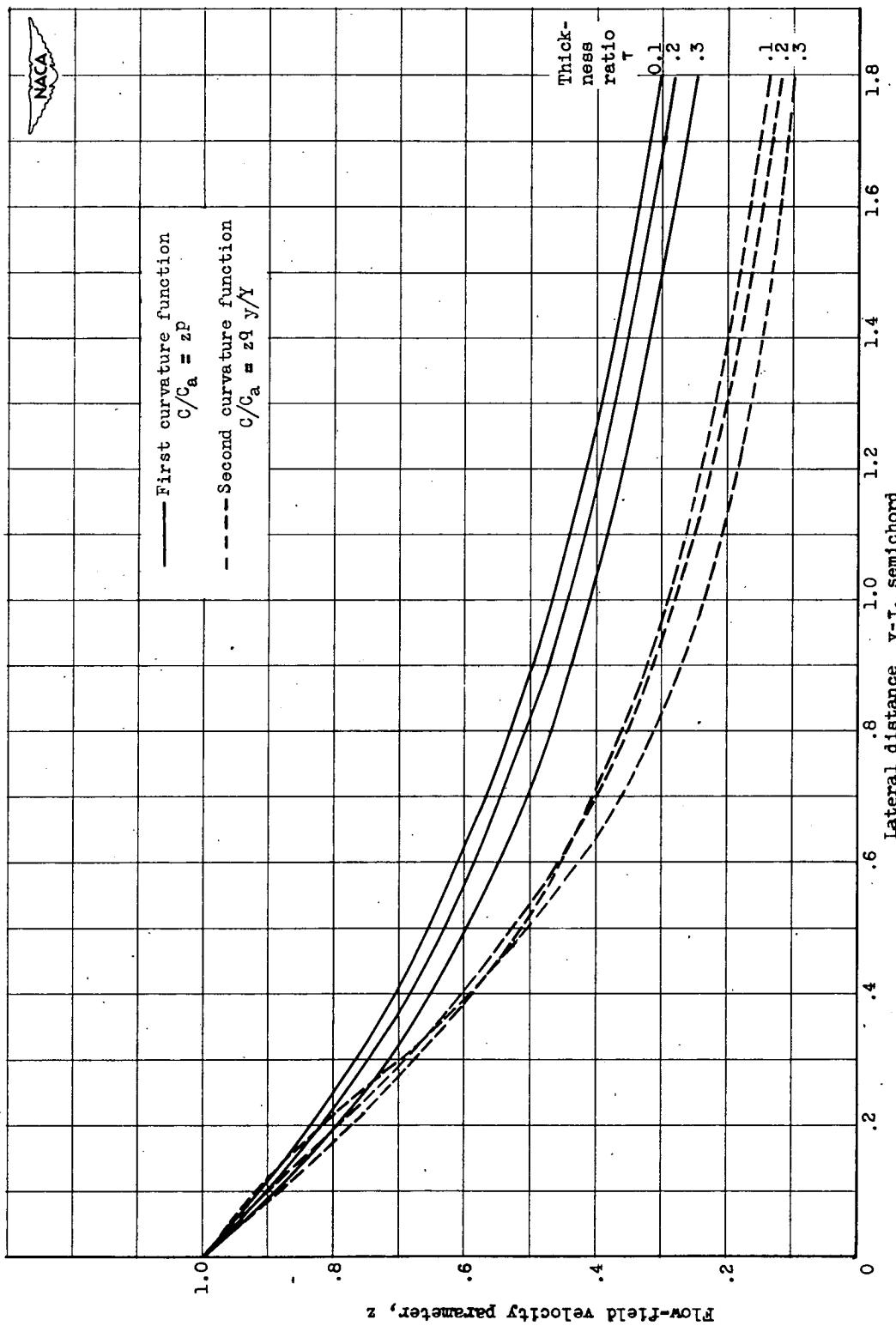
Figure 12. - Lateral variation of velocity in flow field of ellipsoid of revolution at midchord location for potential-limit Mach number and several thickness ratios.
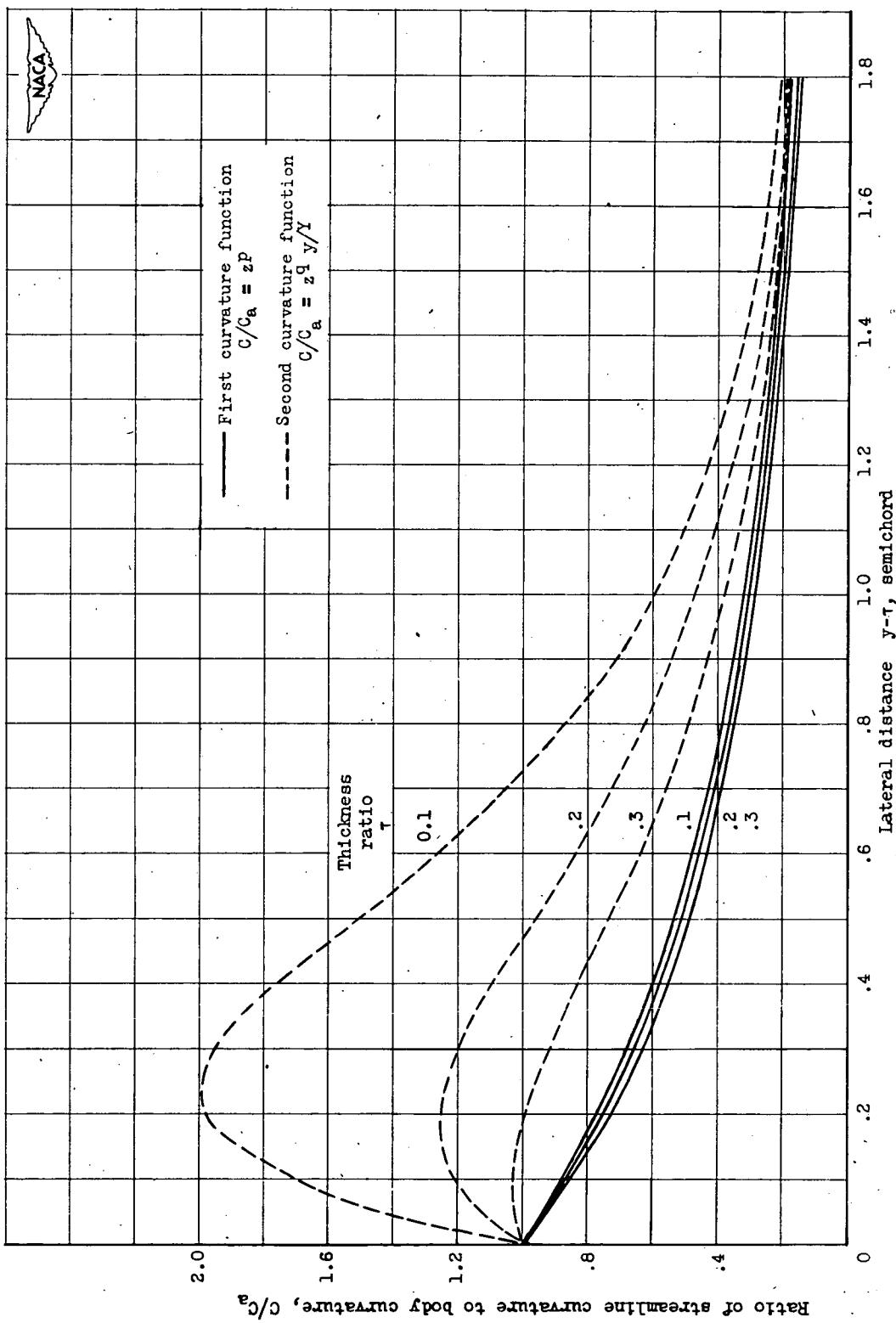
Figure 13. - Lateral variation of streamline curvature in flow field of ellipsoid of revolution at midchord location for potential-limit Mach number and several thickness ratios.
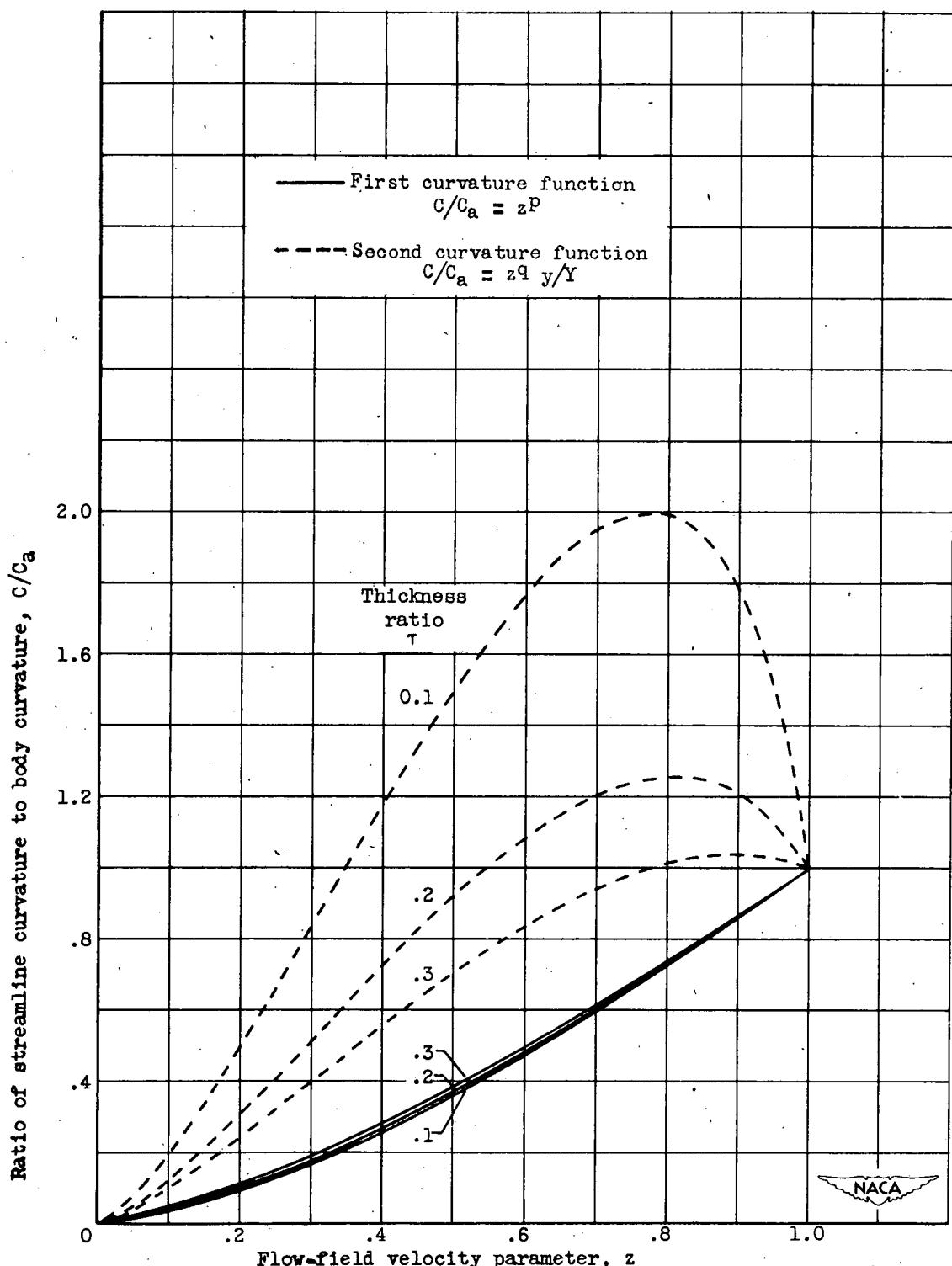
Figure 14. - Variation of streamline curvature with velocity in flow field of
   ellipsoid of revolution at midchord location for potential-limit Mach number
   and several thickness ratios.
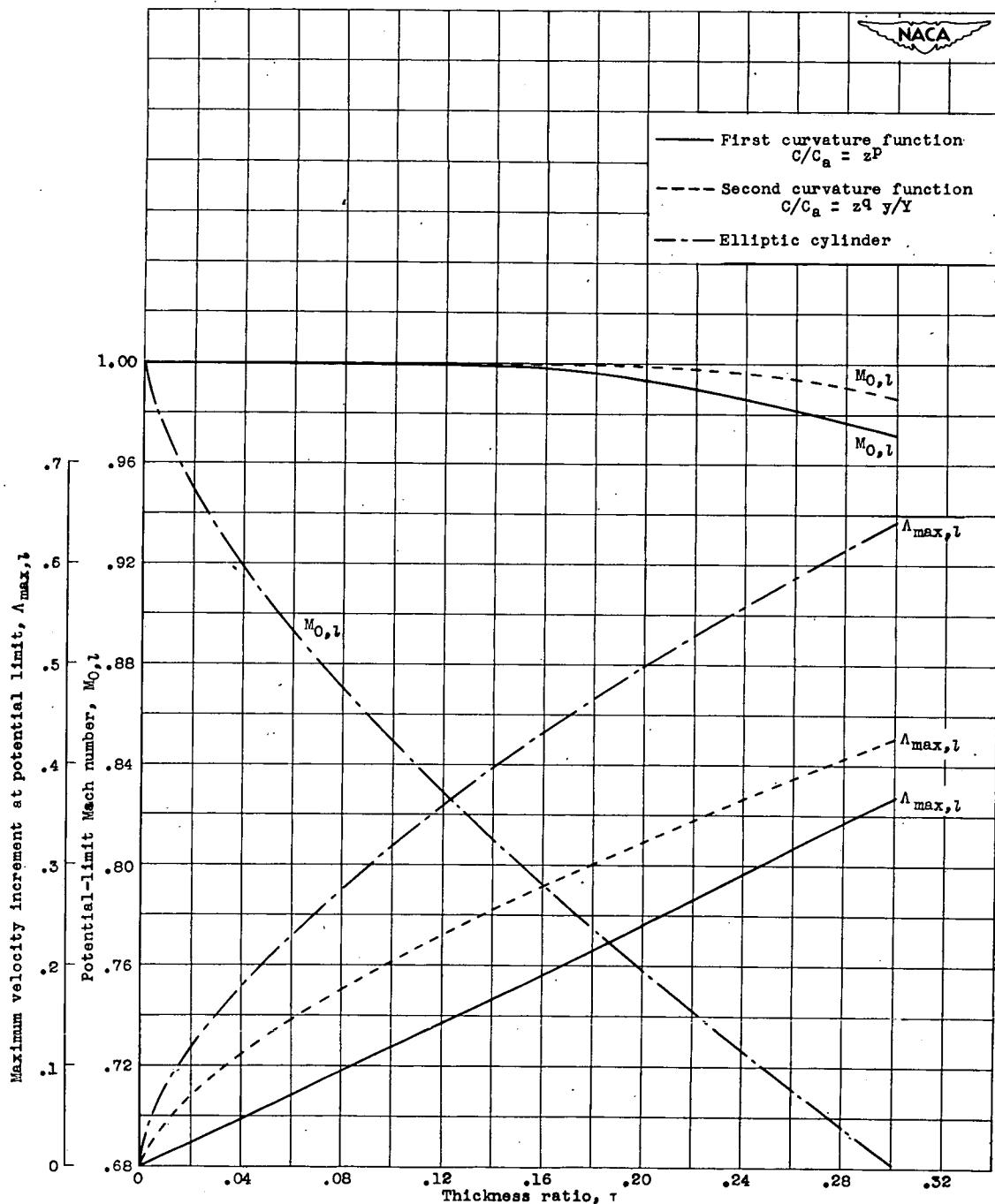
Figure 15. — Potential-limit values of free-stream Mach number and velocity increment at midchord for ellipsoid of revolution and elliptic cylinder as function of thickness ratio.

First curvature function
$C/C_a = zP$

Second curvature function
$C/C_a = zq \ y/Y$

Elliptic cylinder

$M < 1$ $M > 1$ $y_s - \tau$

ξ_s

Longitudinal extent of supersonic region, ξ_s

Lateral extent of supersonic region, $y_s - \tau$

ξ_s

ξ_s

$y_s - \tau$

$y_s - \tau$
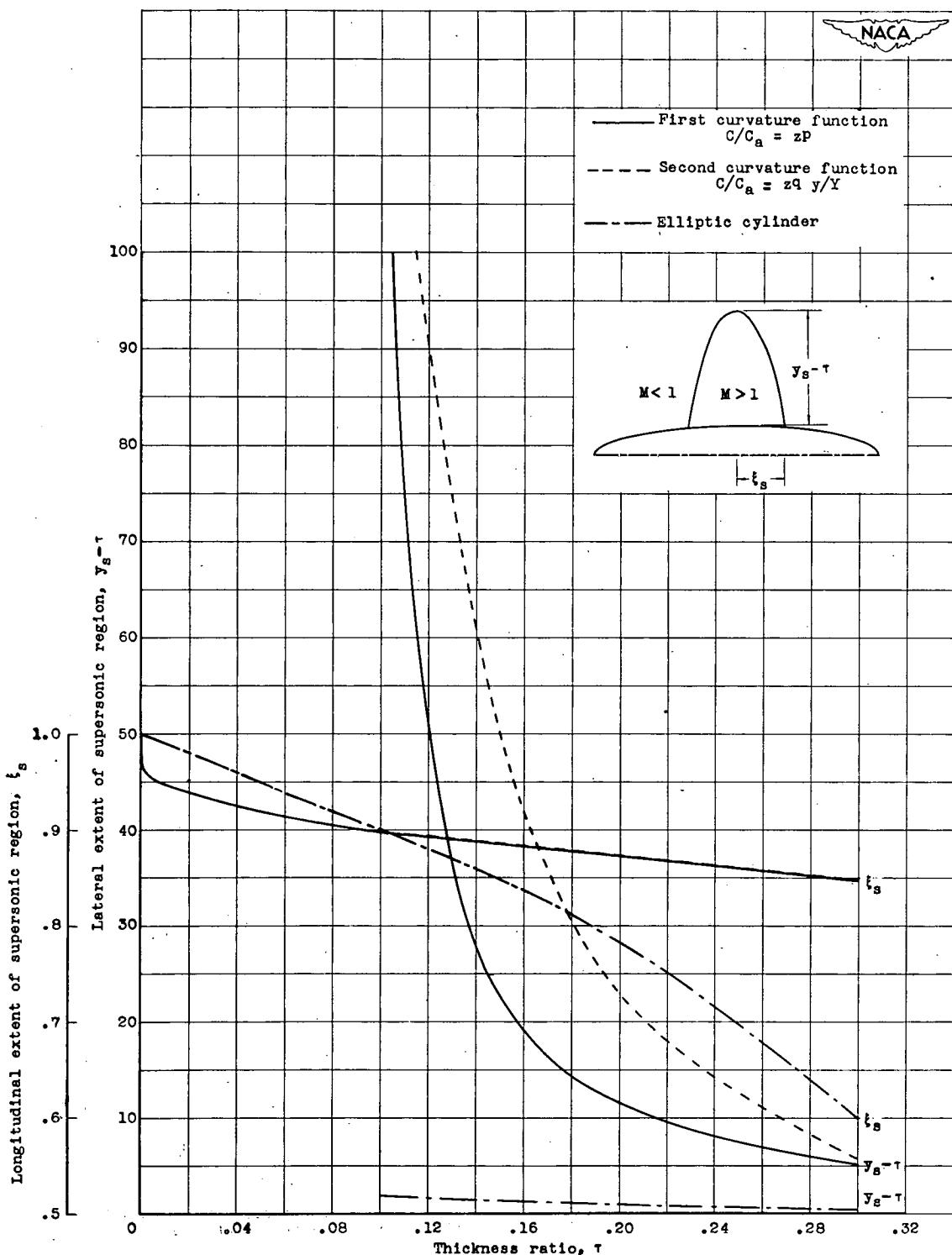
Thickness ratio, τ

Figure 16. - Lateral and longitudinal extents of supersonic region at potential limit for ellipsoid of revolution and elliptic cylinder as function of thickness ratio.